Title
HEAT TRANSFER TO FLOWING GAS-SOLIDS MIXTURES IN A VERTICAL CIRCULAR DUCT

Author
Depew, Creighton Arthur.

Publication Date
1960-07-11

UCRL 9280

UNIVERSITY OF CALIFORNIA

Ernest O. Lawrence

Radiation Laboratory

HEAT TRANSFER TO FLOWING GAS-SOLIDS MIXTURES IN A VERTICAL CIRCULAR DUCT

DISCLAIMER

UCRL-9280
UC-34 Physics and Mathematics
TID-4500 (15th Ed.)

UNIVERSITY OF CALIFORNIA
Lawrence Radiation Laboratory
Berkeley, California

Contract No. W-7405-eng-48

HEAT TRANSFER TO FLOWING GAS - SOLIDS MIXTURES IN A VERTICAL CIRCULAR DUCT

Creighton Arthur Depew

(Thesis)

July 11, 1960

Printed in USA. Price $2.25. Available from the
Office of Technical Services
U. S. Department of Commerce
Washington 25, D.C.

HEAT TRANSFER TO FLOWING GAS-SOLIDS MIXTURES IN A VERTICAL CIRCULAR DUCT

Contents

HEAT TRANSFER TO FLOWING GAS - SOLIDS MIXTURES IN A VERTICAL CIRCULAR DUCT

Creighton Arthur Depew
(Thesis)

Lawrence Radiation Laboratory
University of California
Berkeley, California

July 11, 1960

ABSTRACT

The problem of heat transfer to an air stream laden with solid spherical particles flowing up a vertical tube with constant heat flux was examined analytically and experimentally. Two different particle sizes were used, 30 microns and 200 microns in diameter. The air rate was held constant at Reynolds number = 13,500 and 27,400 while solids were added up to gravimetric ratios of seven.

The analytical treatment parallels the solution for single-phase flow. An approximate solution is obtained when it is assumed that the difference in the temperature of the two phases is small, and that the radial temperature profiles of the two phases in the fully developed region are similar. Nusselt numbers are based on the local tube wall and bulk mean mixture temperatures. Qualitative agreement with the experimental results is obtained.

The analysis predicts that when solid glass particles are added to the air stream in increasing numbers, the asymptotic Nusselt number decreases to a minimum and then increases. The experimental results show that the Nusselt number remains constant for loading ratios less than 0.5 and decreases to a minimum which occurs between 1.0 and 1.5. The length of the thermal entry region increases with increasing solids to gas ratios and was found to be longer than the heat transfer tube (46.4 pipe diameters) at a loading ratio of unity. Although the analysis predicts an increasing Nusselt number at ratios greater than 2, the

experiments with 200-micron particles show that the Nusselt number is independent of the solids loading.

Friction factors calculated from overall pressure drop measurements predict heat transfer coefficients, according to Reynolds analogy, that agree with experimental values within 20% for solids loadings less than 0.5.

I. INTRODUCTION

The technique of transporting finely divided solid materials by fluid suspension has been used widely for a number of years. Though the particle-fluid interactions are not well understood, systems have been designed and operated continuously. If the duct that is transporting the mixture is heated, the picture is complicated by the energy exchange phenomenon. Waste heat boilers recovering energy from flue gas–catalyst mixtures in the petro-chemical industry are an example of an industrial use. Here again, the application did not demand a complete understanding of the mechanism, but the increasing number and complexity of applications–particularly in the fields of solid propellant combustion and nuclear reactor cooling–have added impetus to the search for fundamental knowledge about the heat transfer mechanism.

A. Previous Analytical Work

S. L. Soo and others[15, 16, 17] have used the statistical theory of turbulence to investigate various statistical properties of isothermal two-phase flow. Their system is generally confined to flows characterized by isotropic turbulence and particle motions having Reynolds numbers less than 1.

Soo's early work[15] on momentum transfer in two-phase isotropic turbulence shows that the scale of turbulence of the particles is always greater than that of the continuous phase and that the intensity of turbulence of the particles is less than the main stream. The ratios of fluid-particle intensity and particle-fluid scale of turbulence are zero for very small sizes, and increase with increasing diameter. Soo shows that the ratio of particle to fluid diffusivity is always equal to or greater than unity (cf. his Fig. 2). Further work by Soo and Tien[17] indicates that this ratio is shown to be always unity (see Appendix 6, Reference 17). Because the ratio of diffusivities is independent of particle size, small particles should be used in heat transfer systems to provide favorable particle surface to volume ratios.

This analytical study lends a great deal of understanding to the turbulent properties, but the real effects due to the presence of the wall as found experimentally by Soo and Ihrig[16] are of considerable importance. An analytical treatment of this effect was performed by Soo and Tien.[17] Among their important results are:

(1) particle intensity increases towards the wall, but the particle scale of turbulence decreases;

(2) statistical properties are affected by the wall more at lower pipe Reynolds numbers than at higher Reynold numbers;

(3) intensity of motion of the particles relative to the fluid intensity approaches zero as the particle size increases.

The above analytical treatments neglect the action of one particle on another. Peskin[11] has considered the case of a single particle suspended in a turbulent fluid including the pressure forces due to the motion of similar particles. His results differ from Soo and Tien[17] in finding that the ratio of particle diffusivity to fluid diffusivity is less than unity and decreases with increasing size.

Lumley[6] has derived the complete equations for the particle motion, but these are left in unsolved condition because of their complexity.

Statistical properties of turbulence have not been applied quantitatively with a great measure of success to ordinary physical systems, and this is no less the case in two-phase motion. The qualitative effect of these statistical properties on the bulk transport properties is the most that can be expected from the statistical theory at the present time. These analyses always assume a precise specification of the continuous phase properties and ask the question- if the fluid motion is known, what is the motion of the particle relative to the continuous phase? Since it is logical to presume that the heat is transferred first to the fluid—neglecting radiation from wall to solids–and secondly from fluid to solids, the question that is more pertinent (and more difficult to answer) is - what is the effect of solid particles on the fluid phase motion?

Tien[20] has made the first analytical attempt to predict the effect on heat transfer of adding solid particles to an air stream. It was necessary to make many assumptions to make the system mathematically tractable. Some of the most important assumptions are the following:

(1) the solid phase is uniformly distributed over the pipe cross-section;

(2) the heat transfer coefficient between the solid and fluid phases is uniform and constant;

(3) the time average relative velocity between the two phases is zero;

(4) the solid phase has no effect on the continuous-phase velocity distribution.

The fourth assumption restricts the model to lean mixtures. A solution is obtained for the isothermal tube-wall case, which is extended to the case for arbitrary wall temperature variations and wall heat fluxes by the method of Tribus and Klein,[21] and Sellar, Tribus and Klein.[12] The analysis predicts higher average heat transfer coefficients due to prolonged thermal entry lengths. The analysis presented in Appendix D (Theoretical Analysis) of this dissertation follows very closely the technique used by Tien.

B. Previous Experimental Work

The first experimental work on heat transfer to flowing gas-solids mixtures was done by Farbar and Morley.[4] Their system consisted of alumina-silica catalyst particles, suspended in an air stream, flowing in a vertical isothermal tube. The dispersed phase ranged in size from sub-micron to 200 microns. Overall heat transfer coefficients based on logarithmic mean gas temperatures are reported to be 300% higher than with air alone at high solids loading ratios. A correlation of their data showed that the gas-phase Nusselt number varies with the solids-to-gas loading ratio to the 0.45 power.

The author[3] performed experiments with solid glass spheres in an isothermal tube apparatus very similar in design to the equipment used by Farbar and Morley. It was found that 200μ diameter spheres had no effect on the overall heat transfer coefficient and even 70μ particles had only a slight effect.

This work was extended to 30μ glass beads. Higher average coefficients, similar to those found by Farbar and Morley, were obtained with the smaller size. For the results of this work, along with a brief description of the experiments, see Appendix C and Fig. 21.

Experiments with an electrically heated tube containing a carbon suspension in nitrogen and helium gases have been performed by the Babcock and Wilcox Company[1] in a rather large-scale effort. The purpose of their investigation was to show that gas suspension coolants could be used in nuclear reactors to obtain very high tube wall heat transfer coefficients. Though they did demonstrate that a large-scale, closed-loop coolant circuit was practical, their system differed from the one being considered in this dissertation by the presence of spiral turbulators in the heat transfer section.

C. Scope and Purpose of this Work

It was found that there are no published measurements nor theory on the local heat transfer in a pipe having a uniform wall heat flux; and yet, all of the above experimental results proved that solid particles had a large effect. It was realized that further work measuring overall effects would yield no further fundamental information.

The purpose of this work is to propose a theory based on a simplified model, and to check this theory with measurements, using an electrically heated tube with solid spherical particles suspended in an air stream.

II. DESCRIPTION OF THE APPARATUS

The flow system is shown diagrammatically in Fig. 1. Air was drawn from the room through a metering nozzle, past a point where solid particles were added, through the heated tube which was followed by an adiabatic section, through a double cyclone separator where the solids were removed, and exhausted back to the room by an Arcowand industrial vacuum cleaner.

There was no difficulty encountered in adding solid particles to the air stream by simply allowing them to flow by gravity from a hopper mounted on platform scales, after which the mixture was turned through 90° in a long radius glass elbow. It was necessary to install a 3/8in. diameter Venturi nozzle immediately preceding the approach section to redistribute the solids which were concentrated on the outside tube wall.

The heated section, shown in Fig. 2, was made of type 304 stainless steel seamless tubing, 0.750 in. o.d. X 0.710 in. i.d. The approach section, heated section, and adiabatic section were separated by Bakelite insulators. Every effort was made during the machining of these pieces to make the transition smooth and uninterrupted. The adiabatic section immediately followed the heated section and was made of the same tubing material.

At 16 positions along the tube, iron-constantan thermocouples (No. 30 gage) were installed on the tube. On one side of the tube, the thermocouples were spot-welded directly onto the tube metal; on the other side, the thermocouples were butt-welded and insulated from the tube metal by 0.001-in. thick Mylar plastic. These two methods of installing thermocouples were used since it was not known beforehand whether the AC heating current would introduce extraneous effects into the thermocouple system (see Reference 10 for a discussion of these effects). It was found that the 1-mil Mylar insulation would not eliminate the error, which amounted to 2 to 3°F. The voltage output of the thermocouple system was recorded on a Brown Electronik single point recorder, 0-5 mv full scale. It was necessary to use an auxiliary filter to eliminate stray AC voltages amplified in the recorder. These readings were checked occasionally with a Leeds and Northrup model 8662 potentiometer.

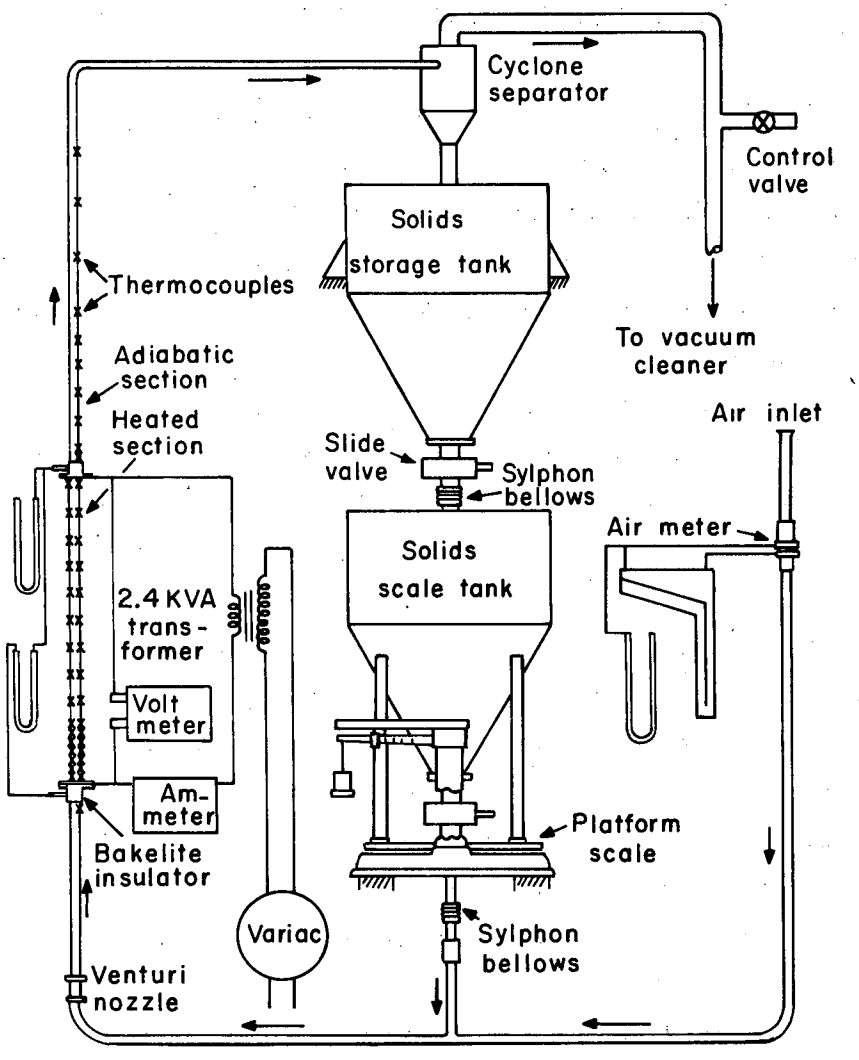

Fig. 1. Schematic diagram of gas-solids heat transfer system.

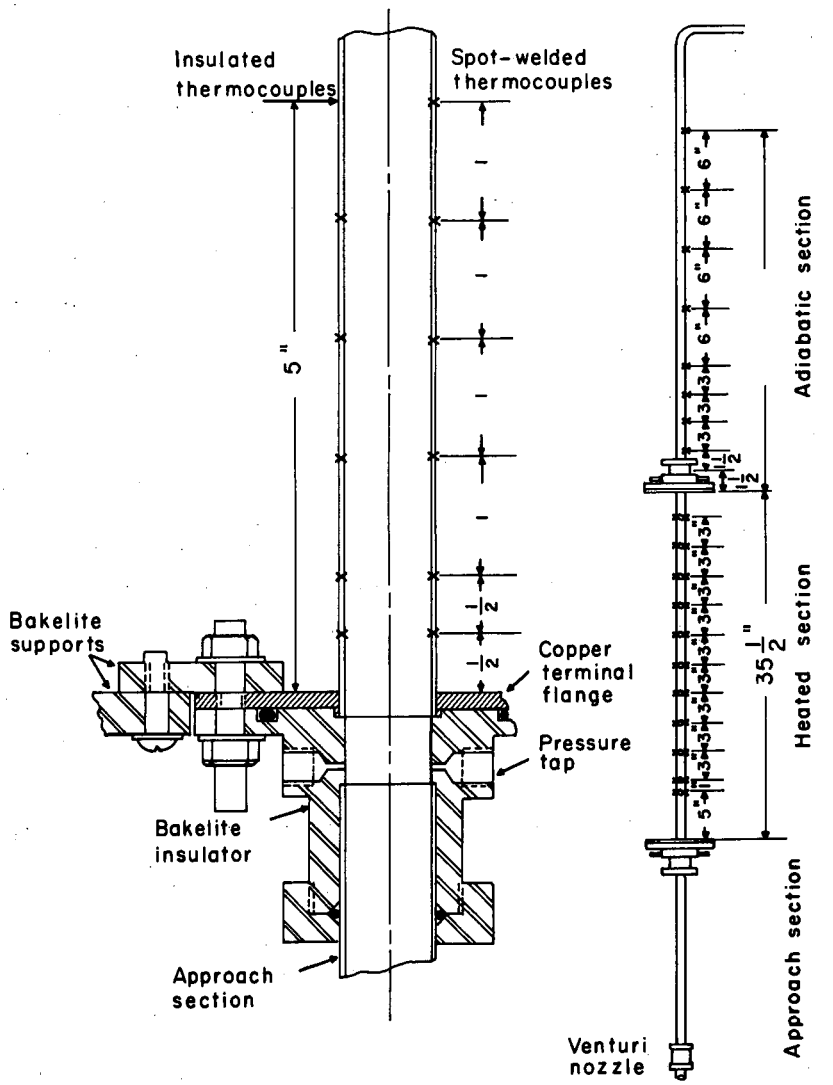

Fig. 2. Detail of test section.

The insulated thermocouples yielded readings that were approximately 3^{o} higher than the spot-welded thermocouples at the same location. In order to determine whether or not the method of installation caused this difference, the method was reversed. At 19-1/2 in. from the inlet, two thermocouples were installed; one thermocouple was spot-welded on the side that had only insulated thermocouples, and one thermocouple was installed on the side where spot-welded thermocouples were used. It was found that the temperature difference was of the same magnitude and in the same direction as in the case of all other locations. It may be concluded that the difference in temperature actually exists, and that it is caused by a non-uniform wall thickness. The tolerance of the wall thickness uniformity is ±0.003 in. It can be shown that only 0.001 in. difference in thickness is necessary to produce this order of temperature difference between one side of the tube and the other. The extraneous AC voltages appeared in each type of thermocouple installation showing that the 1-mil Mylar insulation was not adequate. AC heating current was supplied to the heated section by a 2.4 KVA transformer, controlled on the primary side by a Variac. The two electrical terminal connections at the extremes of the test section were 3-in. diam × 1/8-in. thick copper discs. The copper plates were hard soldered to the tube, thereby producing negligible electrical resistance at the joint. Thermocouples were peened into small holes drilled at radii of 3/4 in., 1-1/8 in., and 1-1/2 in. in the terminal plates, which acted as crude heat meters to indicate heat leak through the copper. The hydrodynamic calming section which preceded the heated tube was 24 in. long (30 pipe diameters) and constructed of the same size tubing as was used in the heated section.

Pressure taps of 1/32-in. diam were drilled through the Bakelite at inlet and outlet to the heated tube, and were connected to manometers. Carbon tetrachloride manometers were used for air alone and low solid concentrations; at high solid concentrations it was necessary to use mercury manometers.

The temperature at the inlet to the heated section was measured by a thermocouple welded to the insulated approach section. Wall

temperatures in the adiabatic section were measured at locations shown in Fig. 2.

The solid particles used in this investigation were glass spheres. Their specific heat (0.191 BTU/lb^{o}F) was determined calorimetrically, and their specific gravity (2.57) was measured by means of a water pycnometer. The manufacturer's* size-specifications were accepted as follows:

Grade Number	Passing U.S. Screen	Passing Opening	Retained on U.S. Screen	Retained on Opening
110	60	250 μ	80	177μ
119	[average bead size = 28μ]			

The largest fraction will be referred to as the 200 μ size and the smallest fraction as the 30 μ size. Fig. 3a-3b is a photomicrograph of both sizes. The pictures show their uniformity of shape. In the remainder of this dissertation, these particles will often be referred to as beads.

*Manufactured by the Minnesota Mining and Manufacturing Co.

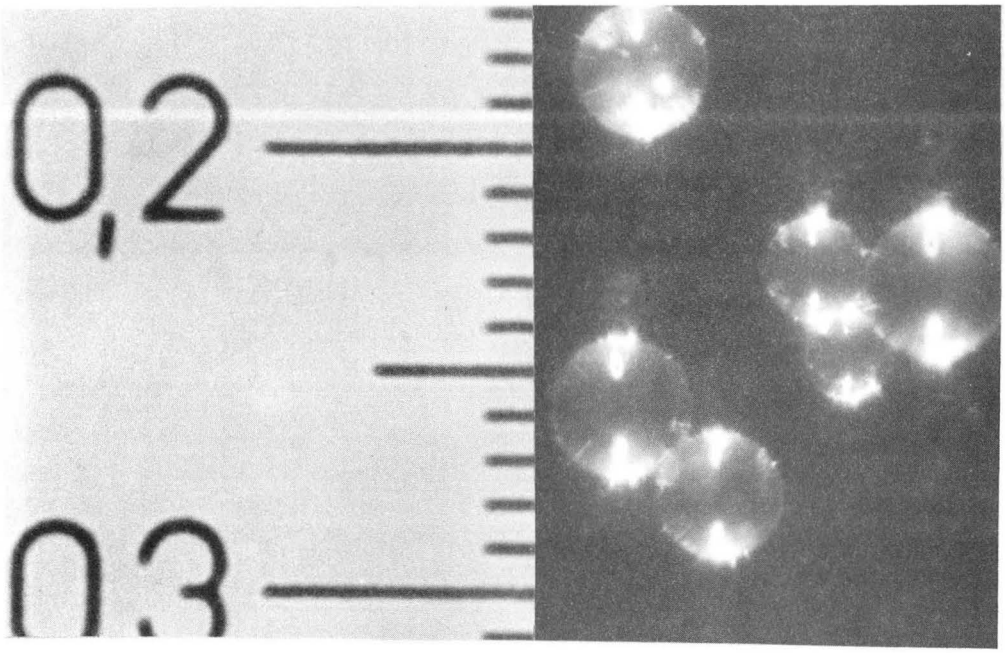

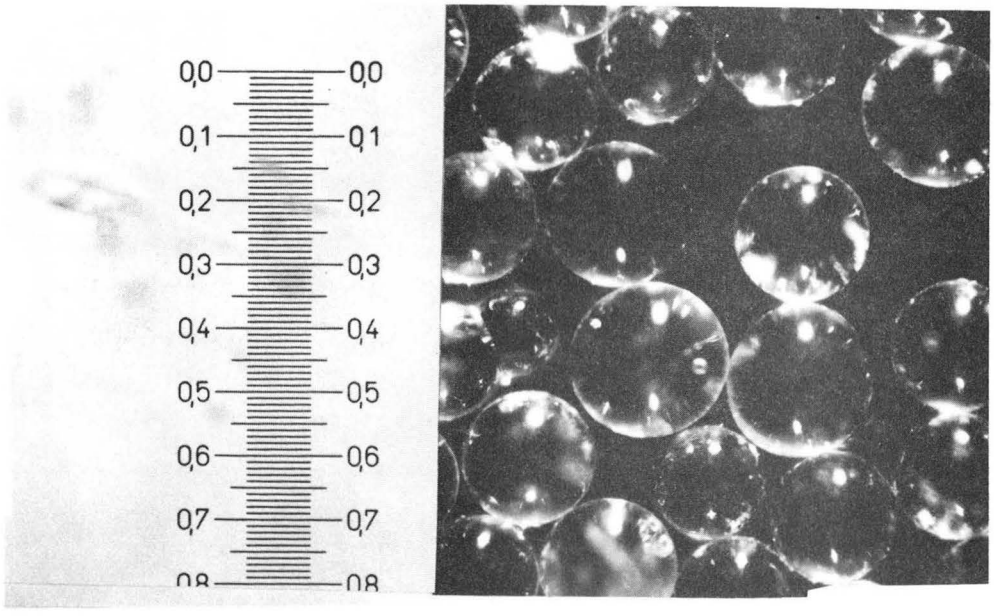

Fig. 3a. 30 micron glass beads (scale indicates millimeters, 1 div. = 10 microns).

Fig. 3b. 200 micron glass beads (scale indicates millimeters, 1 div. = 10 microns).

III. EXPERIMENTAL PROCEDURE

The initial phase of this work was carried out using air alone to check the operation of the apparatus and to determine the heat loss correction that was applied to the measured heat input. These results were compared to existing experimental data and theoretical analyses. The thermal entry temperature solution was measured in the adiabatic section as suggested by Sparrow[18] and compared to the measurements made in the entry section of the heated tube. In all, 24 calibration-runs were made. In addition to the heat transfer calibration, pressure drop measurements were made during this initial period. Pressure drop measurements yielded Fanning friction factors that compared within ± 10% of the expected result.

During the two-hour warm-up period, air rate and power input were set at predetermined values very close to the final desired operating conditions. Temperatures were observed for constancy for about 15 minutes prior to testing. For the air calibration test a wide range of air flow rates was used, but at all times the wall temperature of the outlet of the heated section was maintained at $275^{\circ}F \pm 10^{\circ}$. Each time that a new Reynolds number was desired, the air rate was adjusted, and the power input was reset to yield this temperature. About five minutes was allowed between runs, which was more than adequate considering that the system has a measured 30-second time constant with respect to step inputs of power or step changes in air rate. When steady state was established, current, voltage, pressure drop, thermocouple readings, and air rate were recorded.

The operation with solids was quasi-steady since only a finite inventory of solids was available. One hundred-thirty lbs of 30 μ beads and 70 lbs of 200 μ beads were available. The length of possible running time was of course dependent on the solids rate, and hence upon the particular constant air rate and loading ratio being maintained. The minimum time available for the highest solids loading rate was 20 minutes. This was more than adequate to complete a run after steady state was obtained. As a rule, less than five minutes was allowed after conditions were set, and the normal length of time was about two minutes. The usual procedure

when making measurements with solids was to first make a run with air alone, to establish steady state for the experimental period, and then to set an air rate higher than the desired air rate. As solids were added the air rate decreased, and when a desired solids concentration was obtained, the air rate was adjusted to the constant value. Once steady state was established, all of the above measurements were taken in addition to weight-versus-time readings on the solids scale tank. The inventory of 30 μ beads was run through the system from two to three times during any one testing period. Retention of the heat from the previous test period made the solids warmer than the incoming air. Data on the isothermal tube system in the adiabatic section showed that the 30 μ solids readily came to the same temperature as the gas in a 3-foot length. This information was used to establish the temperature equivalence of the two phases at the inlet of the heated section. It was known, however, that the 200μ particles took a considerably longer distance to come to the temperature equilibrium with the air, so that only one pass through the system was allowed during any one day.

The range of variables used in these experiments includes two constant gas Reynolds numbers: 13,500 and 27,400. Two bead sizes were used, 30 μ and 200 μ. The solids loading ratios were from zero to 3.5 for the high Reynolds number, and from zero to 7.0 for the low Reynolds number.

IV. ANALYSIS OF DATA

The results of this investigation naturally separated into two categories: (1) local heat transfer coefficients, and (2) overall pipe friction factors.

A. Heat Transfer results

The local heat transfer coefficient is defined by the following equation

$$h \equiv \frac{q}{T_0 - T_{mm}}$$

where q is the local pipe wall heat flux, T_0 is the measured pipe wall temperature, and T_{mm} is the mixed mean temperature of both phases. T_{mm} was calculated using an energy balance between heated section inlet and the desired location x by the formula

$$T_{mm} = T_1 + \frac{2\pi q r_0 x}{\overline{W c} + W_s c_s}$$

The measured heat input was corrected by the average heat loss from the central portion of the heated length – assuming this heat loss uniform over the entire length. This correction was nearly constant for all runs, since the system was operated with the tube outlet temperature constant. The amount of the heat loss, 30 BTU/hr, ranged from 1% to 5% of the total heat input, and its determination is shown in detail in Appendix G. The average of the two outside tube-wall thermocouple readings was used for the tube wall temperature. Averaging the two readings gives entirely correct results if variations in physical properties can be neglected. With the ordinary azimuthal variation 3 to 7F encountered, this procedure is justified. The outside wall temperatures were not adjusted for the temperature drop through the tube metal because this correction can be shown to be negligible compared to $T_0 - T_{mm}$ (The conduction drop is 0.14 F at the highest heat flux).

When a major emphasis is placed on local results near the heated tube inlet, it is necessary to show that variations found there are not due to longitudinal heat conduction in the pipe wall or to the lack of a fully established velocity profile. To demonstrate the former, the difference between heat generated per unit of surface area and heat flux to air was computed for the worst case encountered – Re = 13,500. These differences – as percent of heat flux – are 2.7 at 2 diameters, 0.6 at 4 diameters, and 0.3 at 6 diameters. This error is negligible after 2 diameters and approaches zero at the end of the thermal entry length. To answer the former question – was the flow fully developed at the heated section inlet – a drawn brass tube (0.750-in. o.d. X 0.694-in. i.d.) with the Venturi nozzle at its inlet, was set up to measure the local pressure gradient. Pressure taps were 3 in. apart, covering the distance from 4-1/4 in. to 34-1/4 in. from the Venturi outlet. This pressure drop tube was rather crudely constructed and a slight waviness in the wall was observed after the pressure taps were soldered in place. In spite of these variations, and the 2% to 10% error due to the least count of the manometers (0.01 in. water in 0.1 to 0.5 in. measured), conclusions can be made from the tests. The results are plotted in Fig. 24 in terms of pressure gradient vs. dimensionless distance for various solids loading ratios. Fully established flow occurs where the pressure gradient is constant and apparently was not attained at large solids concentrations.

Heat transfer coefficients are reported in terms of the dimensionless Nusselt number or the dimensionless ratio $h(x/D)/h(46.4)$. Physical properties for Nusselt number and Reynolds number are evaluated at the average of the two-phase mixed-mean terminal temperatures, And $h(46.4)$ is evaluated at $x/D = 46.4$ diameters, which is the last measuring point on the tube unaffected by the top terminal flange, and is not necessarily equal to the asymptotic heat transfer coefficient.

B. Pressure Drop Results

If the following assumptions are made for the two-phase mixture:

1. The solid phase is uniformly distributed over the pipe cross-section.

2. The solids and gas velocities are equal.
3. It is assumed that the temperature of the mixture is constant at the average of the two-phase terminal temperatures. This assumption is justified because the deviation of T is less than 12% from the average.
4. The gas phase obeys the ideal gas laws.
5. Gas velocities are much less than the local velocity of sound.

The friction factor for two-phase flow is expressed by the following equation:

$$\frac{4fL}{D} = \frac{\left(\frac{W_s}{W}\right)+1}{G_m^2 R T_{av}} (P_1^2 - P_2^2) - 2 \ln \frac{P_1 T_2}{P_2 T_1}$$

where $f \equiv \tau_0/(\rho_s u_m^2/2g)$

The details of the derivation of this equation are contained in Appendix F.

V. EXPERIMENTAL RESULTS

One of the difficulties that arises in an investigation where local values are measured is the presentation of the large quantity of results. In two-phase heat transfer, the problem is compounded by the presence of another variable, W_s/W. An effort has been made to display these local values clearly; and consequently, it was necessary to omit some results in the graphical work. Where this was done, the results can be safely interpolated between solids loading ratios.

A. System Performance with Air Flow

The acceptable performance of the experimental system was verified by the results of 24 runs with air. The range of Reynolds numbers was from 11,400 to 41,400. Check runs at the two Reynolds numbers that were used with solids were made occasionally throughout the program to ensure the constancy of the system characteristics.

Asymptotic Nusselt numbers are compared with the experimental and analytical results of various investigators in Fig. 4 (the results of Hartnett[5] are not shown since they agree with the Dittus-Boelter correlation to within 10%). The experimental results agree to ± 5% with Sparrow's analytical expression.

$$Nu = 0.0245 \ Re^{0.77}$$

Tabulated values of the asymptotic heat transfer coefficient appear in Table I.

The variation of local heat transfer coefficient with axial distance is tabulated in Table II and shown graphically in Fig. 5. Comparison with Sparrow's analytically determined profiles shows good agreement. Because of the asymptotic approach of Nu to Nu_∞ and experimental error, the precise length of the thermal entry region cannot be accurately determined. A much better criterion for specifying the end of the thermal entry region is the 5% Nusselt number ratio, i.e., where $Nu(x) / Nu_\infty = 1.05$.

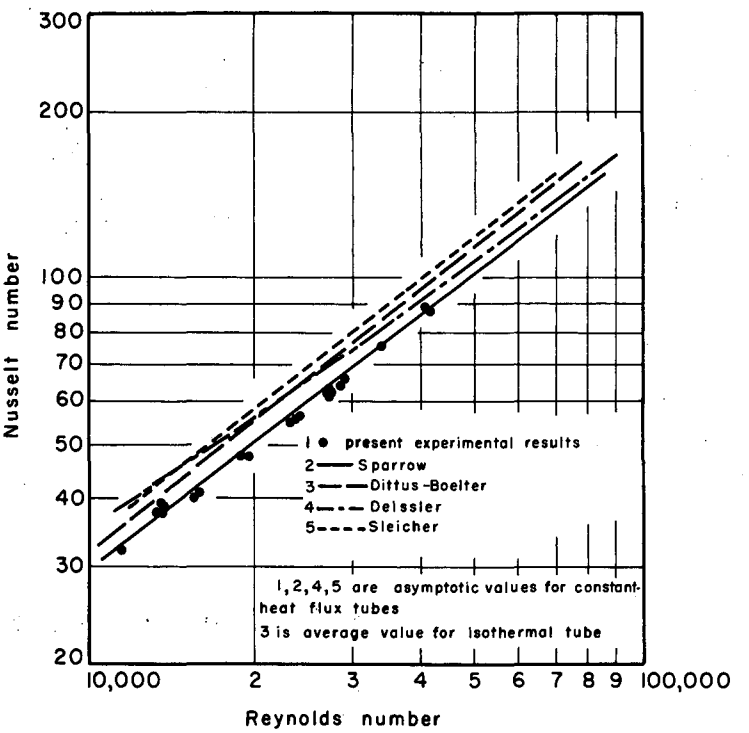

Fig. 4. Nusselt number for air alone vs. Reynolds number.

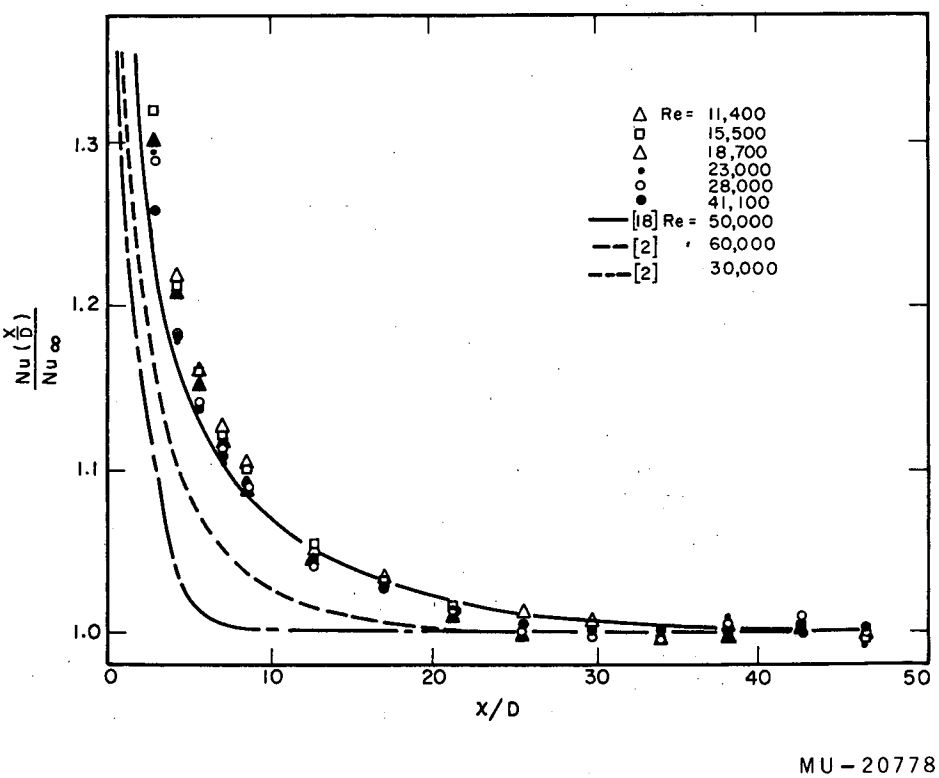

Fig. 5. Local Nusselt number ratio for air alone vs. axial distance.

The values found in Fig. 5 range from 11 to 13 pipe diameters. The entrance region contribution to temperature $\theta_2(x_1^+ r_0^+)$ (see Appendix E for a discussion of θ_2) appears in Fig. 25 and is tabulated in Table IV. It is seen that the values for $\theta_2(\chi^+ \nu_0^+)$ in the adiabatic section are only about half those in the heated section. The reason for this poor agreement is probably due to the large thermal gradient – which is due to heat-leak through the end fittings –in the heated tube within a few diameters of the top terminal flange.

Overall pressure drop measurements are reported in terms of the Fanning friction factor in Table III and in Fig. 6. The results with the heated tube scatter uniformly over the range of Reynolds numbers encountered. With the exception of one point, they fall within ± 10% of the recommended curve. The scatter in these results is due to the low precision of the manometers, which allowed a maximum error of 16% at low air rates and 6% at high air rates. At the completion of all of the heat transfer experiments, pressure drop measurements were made on the unheated tube with inclined manometers, giving maximum errors of 3% and 2% at the low and high rates respectively. These results are plotted in Fig. 6 and are more consistent than the previous results. The points fall 5% below the recommended curve at high rates and increase, relative to the curve, to 10% higher than the curve at the lowest air rate.

B. Gas-Solids Heat Transfer Performance

The dimensionless tube wall temperature vs. axial distance is shown for various representative solids loadings in Figs. 7, 8, 9, and 10. These curves indicate the greater effectiveness of the two-phase mixture in cooling the wall compared to the air flow alone. One exception to this effect is seen with 30μ particles at Re = 13,500 for W_s/W less than unity. For these conditions the heat flux required to maintain the same wall temperature was less with solids than without solids. The 200 μ beads had little or no effect even at high loading ratios.

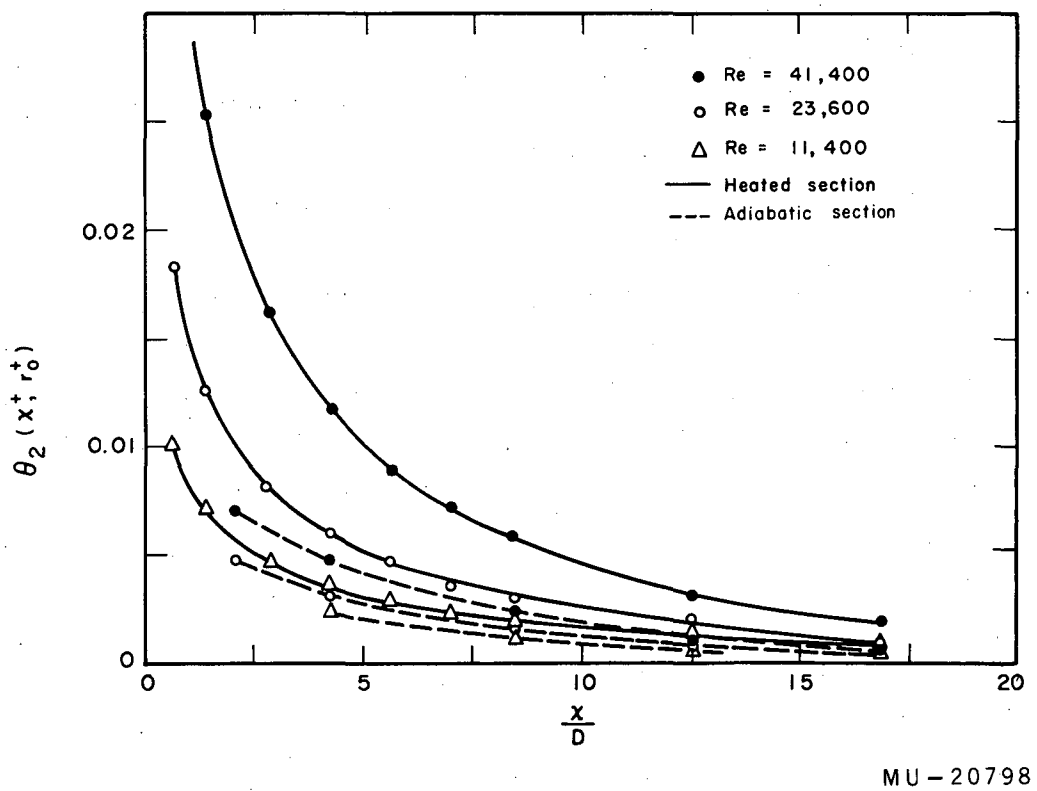

Fig. 25. $\theta_2 (X^+, r_0^+)$ vs. axial distance for air.

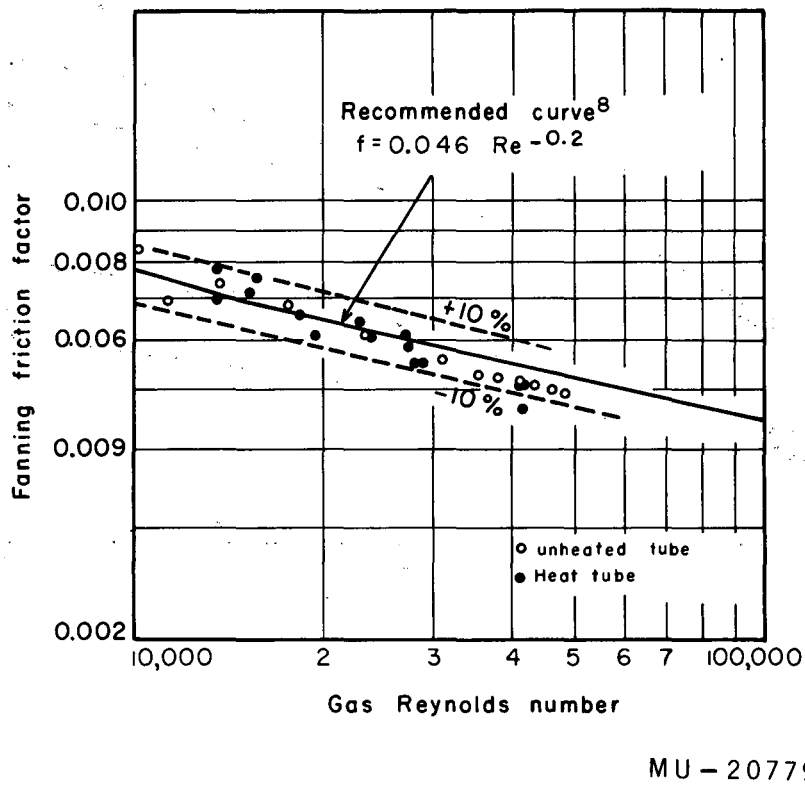

Fig. 6. Friction factor for air alone vs. Reynolds number.

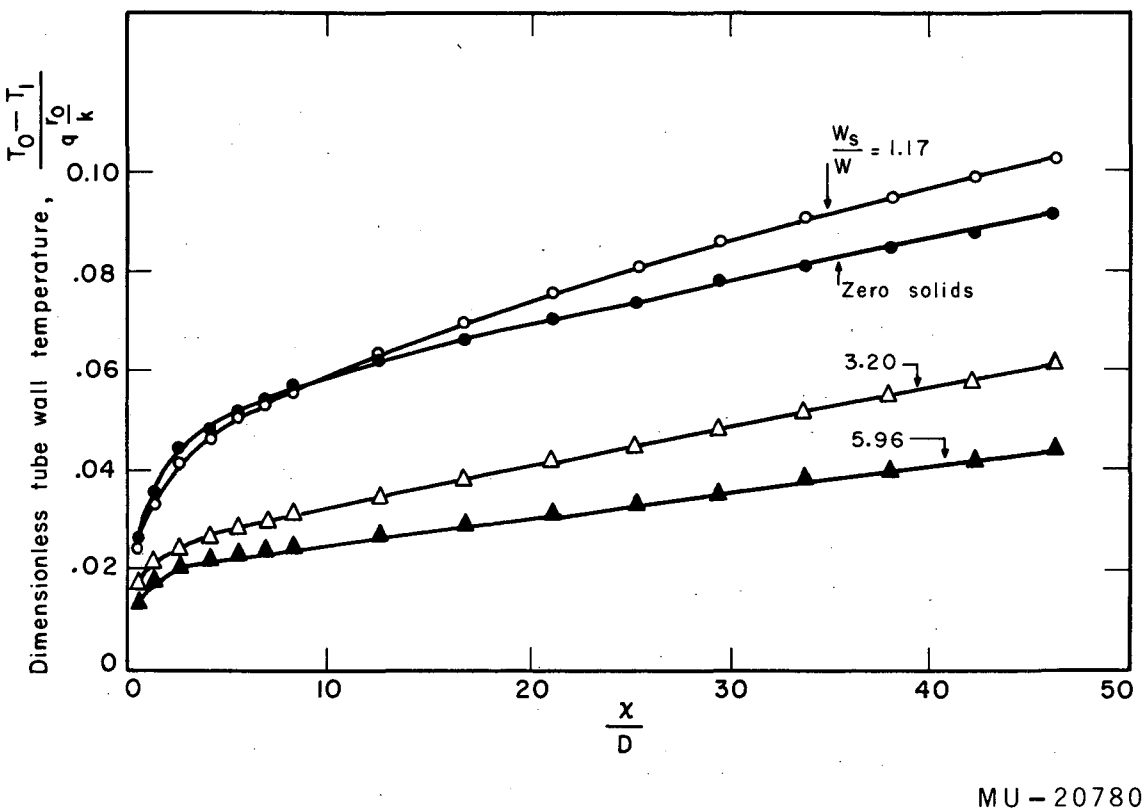

Fig. 7. Dimensionless tube wall temperature vs. axial distance for 30μ particles, Re = 13,500.

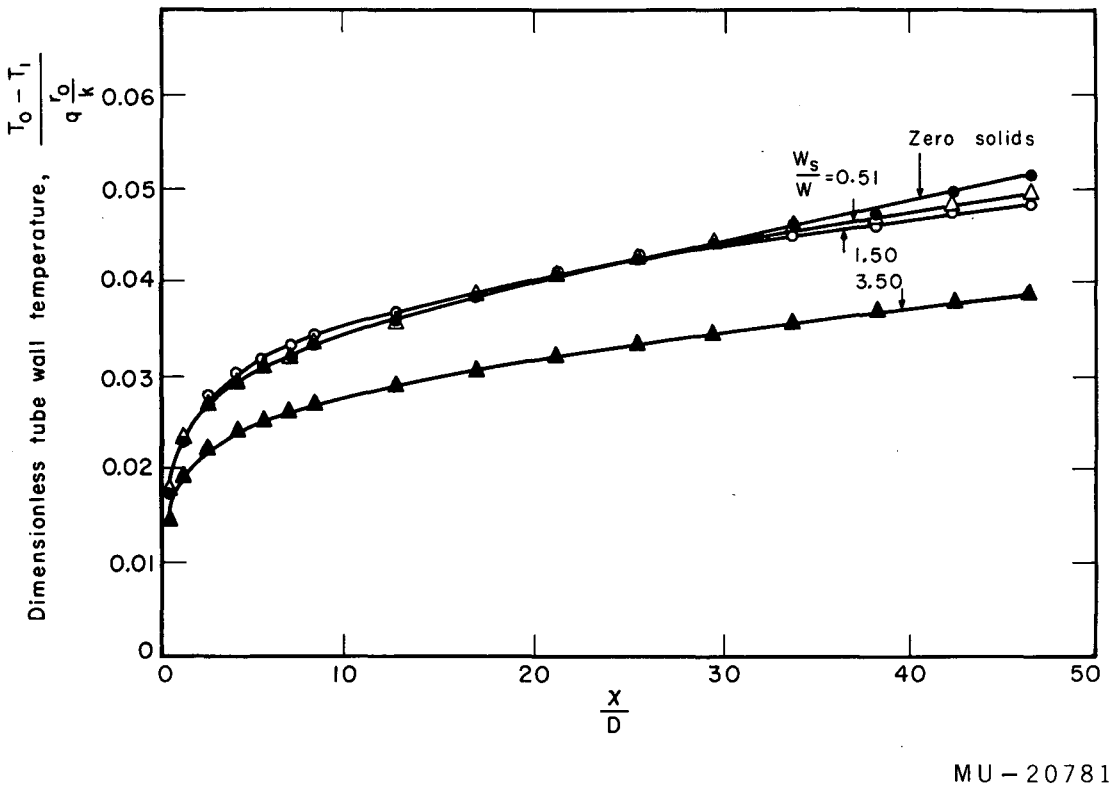

Fig. 8. Dimensionless tube wall temperature vs. axial distance for 30μ particles, Re = 27,400.

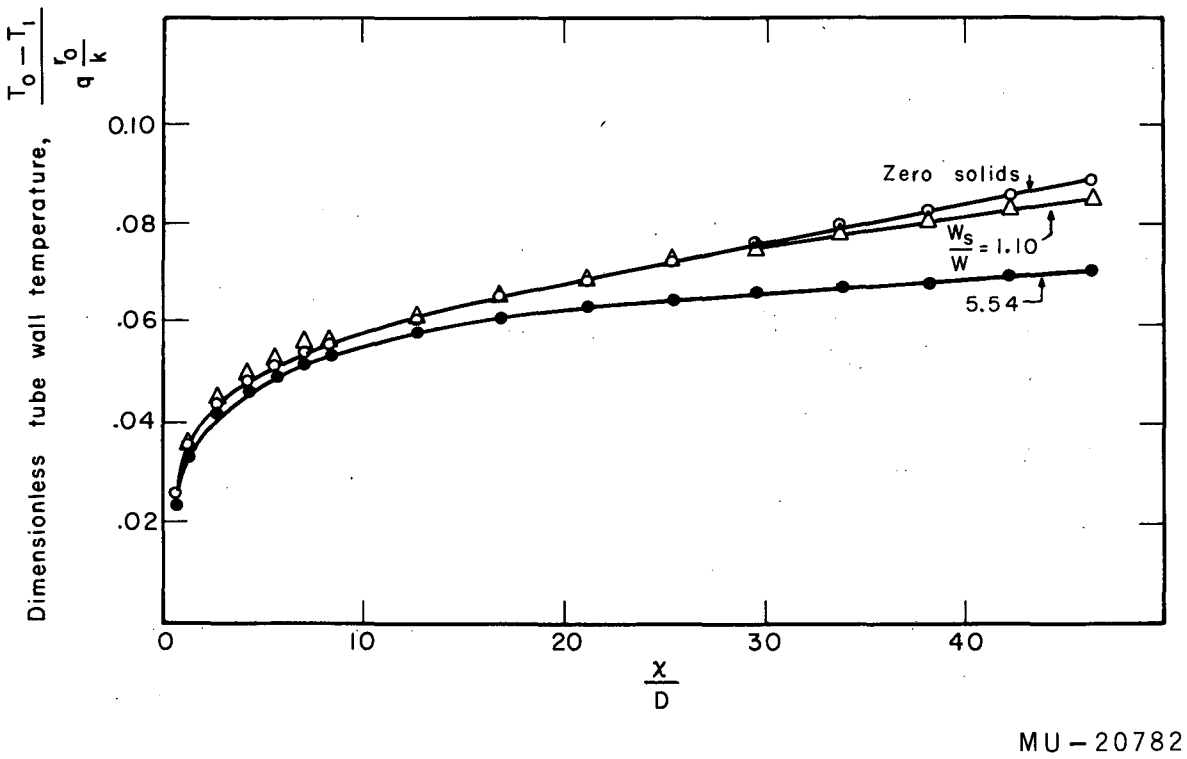

Fig. 9. Dimensionless tube wall temperature vs. axial distance for 200μ particles, Re = 13,500.

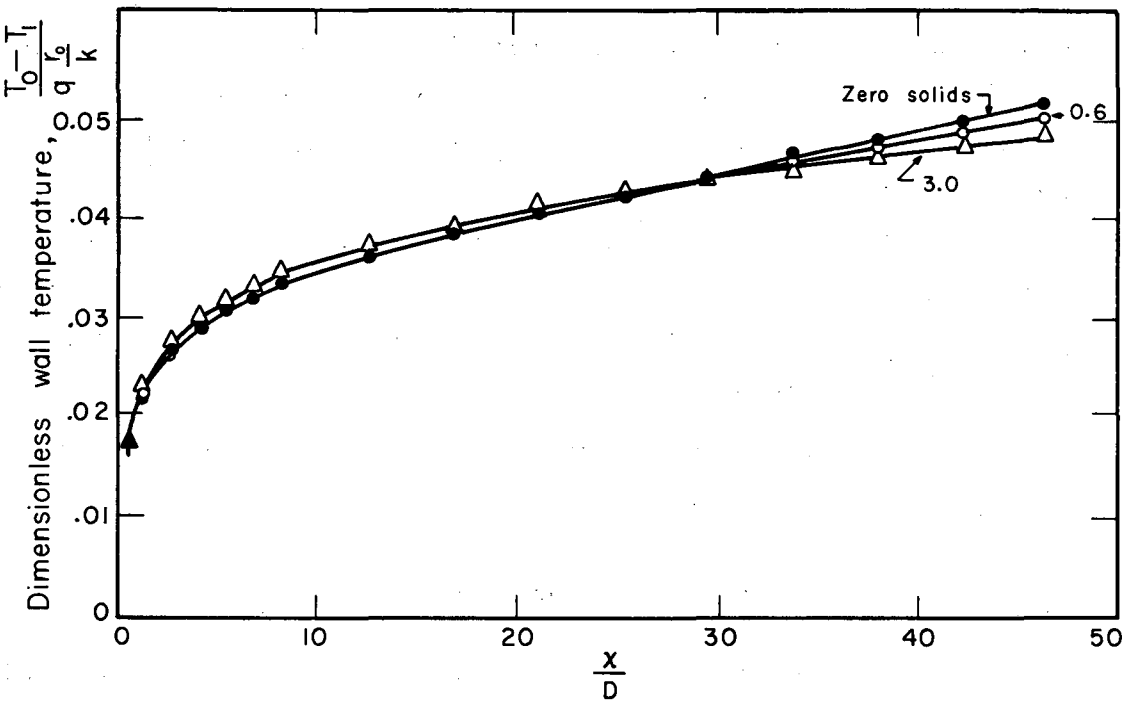

Fig. 10. Dimensionless wall temperature vs. axial distance for 200 μ particles, Re = 27,400.

Tube wall heat transfer coefficients, as obtained in the manner shown in Analysis of Data, are shown in the form of Nusselt numbers in Figs. 11 and 12 for three locations in the heated section. The general shape of the curves in Fig. 11 is the same for all three locations at both Reynolds numbers. For loadings less than 0.5, Nu is unaffected; at higher loadings, the curves pass through a minimum and then increase regularly. The results using 200 μ particles (Fig 12) are quite different; there is practically no effect due to the solids. At the lower velocity, a slight decrease occurs between 0.5 and 1.0; when the loading ratio is greater than unity, the Nusselt number is again constant.

The local Nusselt numbers are again presented in terms of the ratio $Nu_s/Nu_s(46.4)$, where $Nu_s(46.4)$ is the value obtained at $x/D=46.4$. These curves, shown in Figs. 13, 14, 15, and 16, are compared to the analytically predicted ratio Nu_s/Nu_∞.

The length of the thermal entry region increases as solids are added to the air stream.

C. Gas-Solids Pressure Drop

Pressure drop through the heated section vs. solids loading ratio is shown in Figs. 17 and 18 for the two bead sizes. The mixture of 200 μ glass spheres exhibits a linear pressure drop relationship with loading, but the curve that was obtained with the smaller size undergoes a slight upward curvature.

The calculated Fanning friction factors are presented in Tables IX and X, and are shown in Figs. 19 and 20. Similar to the heat transfer results, the curves decrease with loading, but here the decrease begins immediately with even very lean mixtures. Only in one case – 30μ spheres at Re = 13,500 – was a minimum observed.

D. Heat Transfer in an Isothermal Tube with 30-micron Particles

Experiments were made in an isothermal tube in the manner described in Reference 3 (see Appendix C for a discussion of these tests).

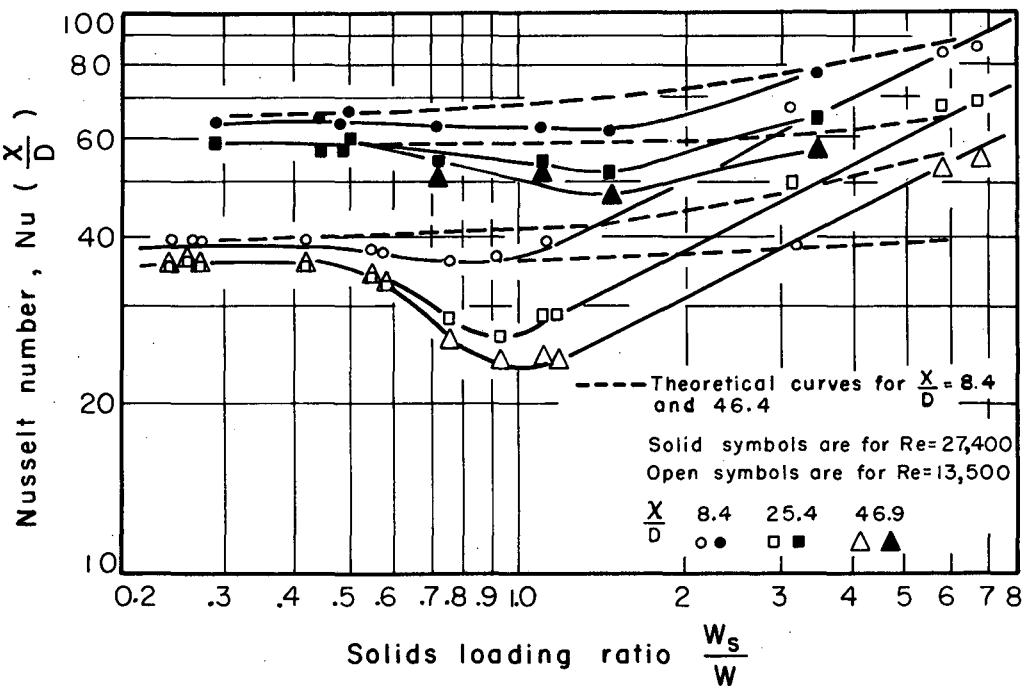

MU-20784

Fig. 11. Local Nusselt number vs. solids loading ratio, using 30μ particles.

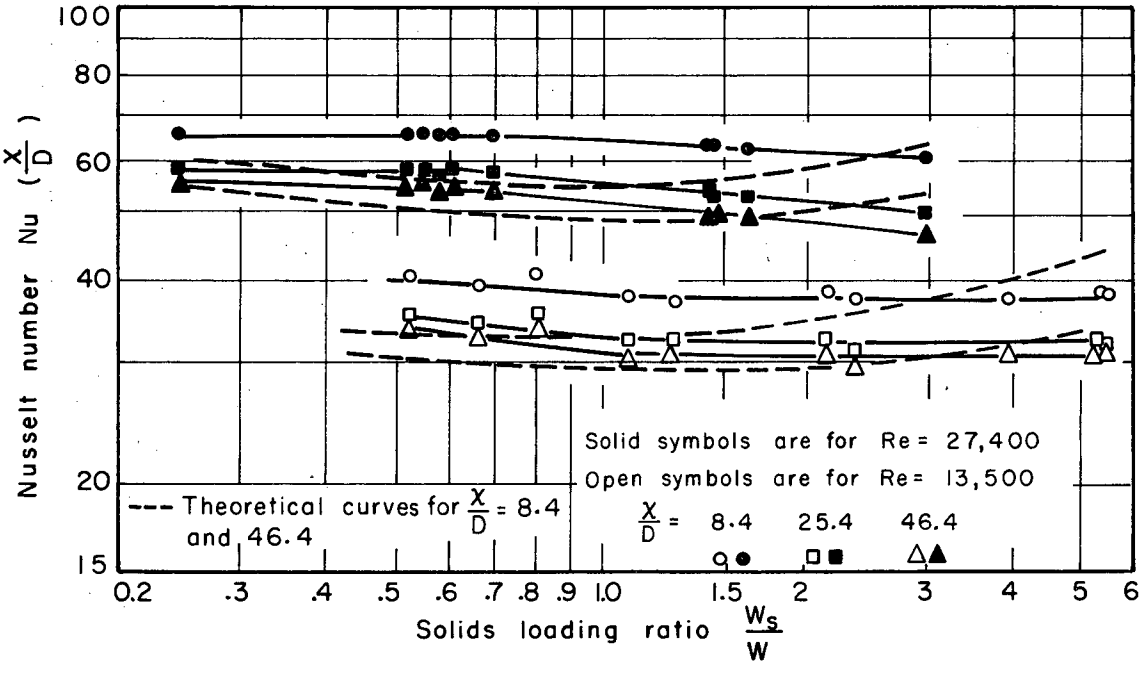

Fig. 12. Local Nusselt number vs. solids loading ratio, using 200μ particles.

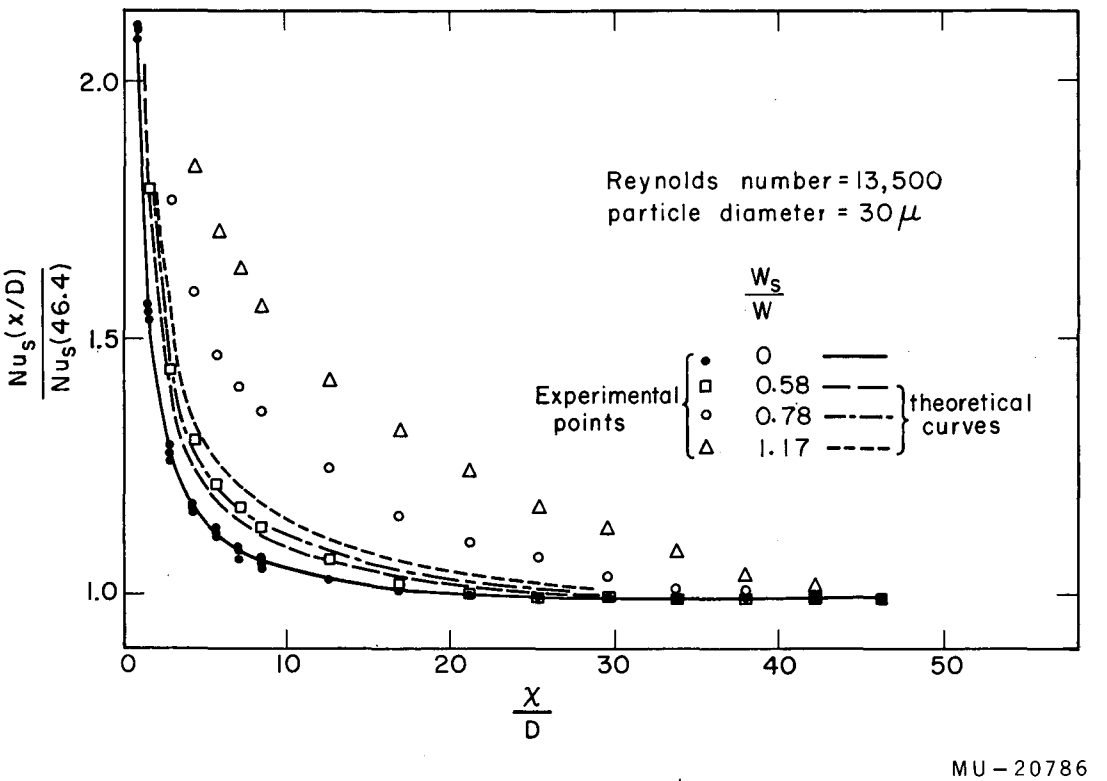

Fig. 13. Local Nusselt number ratio vs. axial distance at different loading ratios.

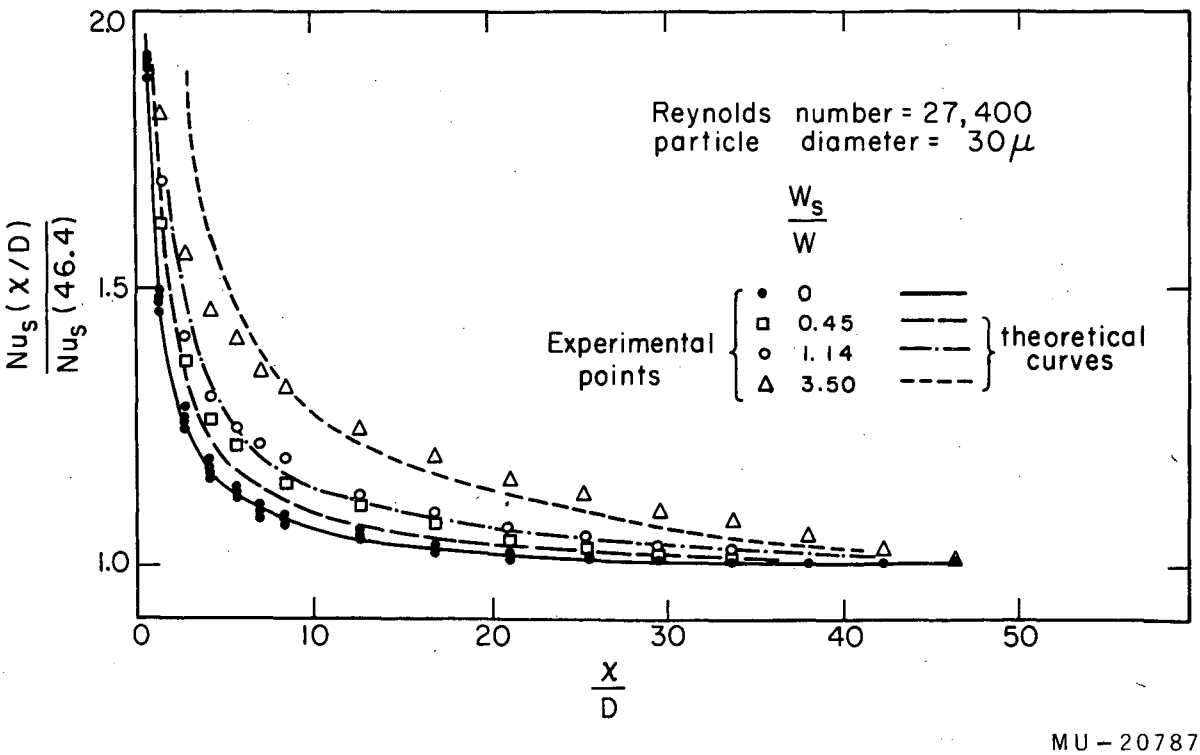

Fig. 14. Local Nusselt number ratio vs. axial distance at different loading ratios.

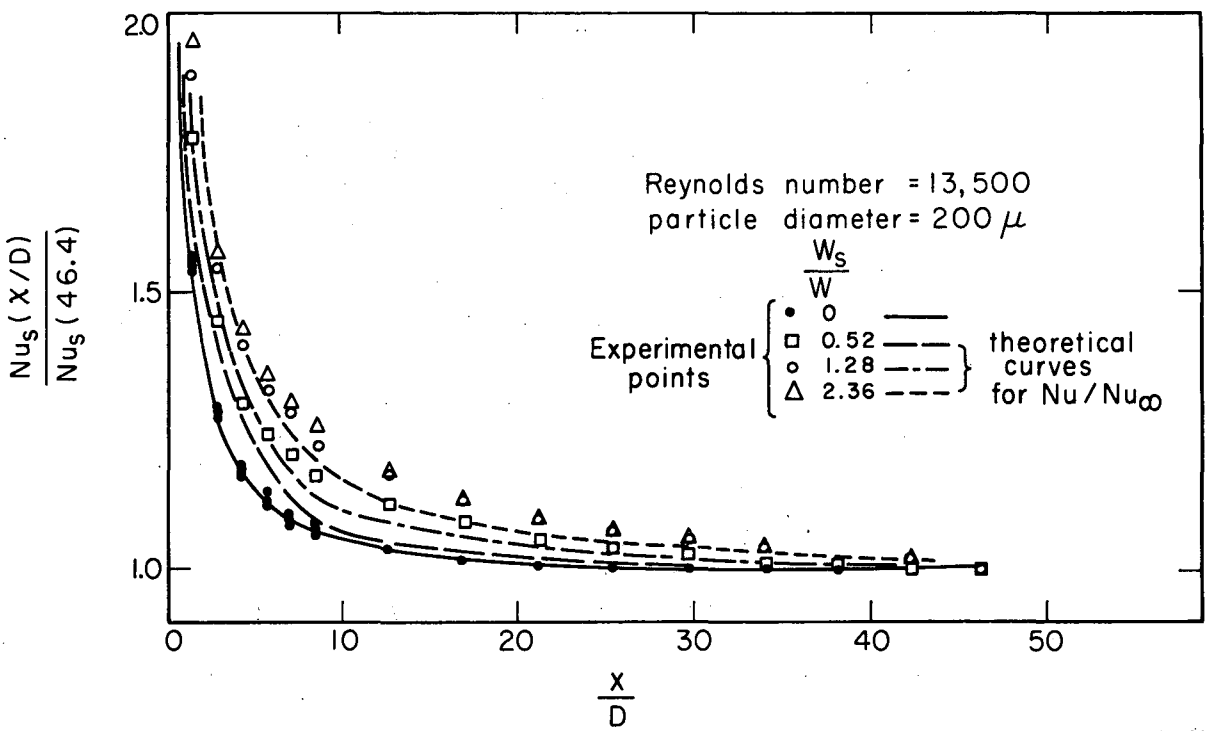

Fig. 15. Local Nusselt number ratio vs. axial distance at different loading ratios.

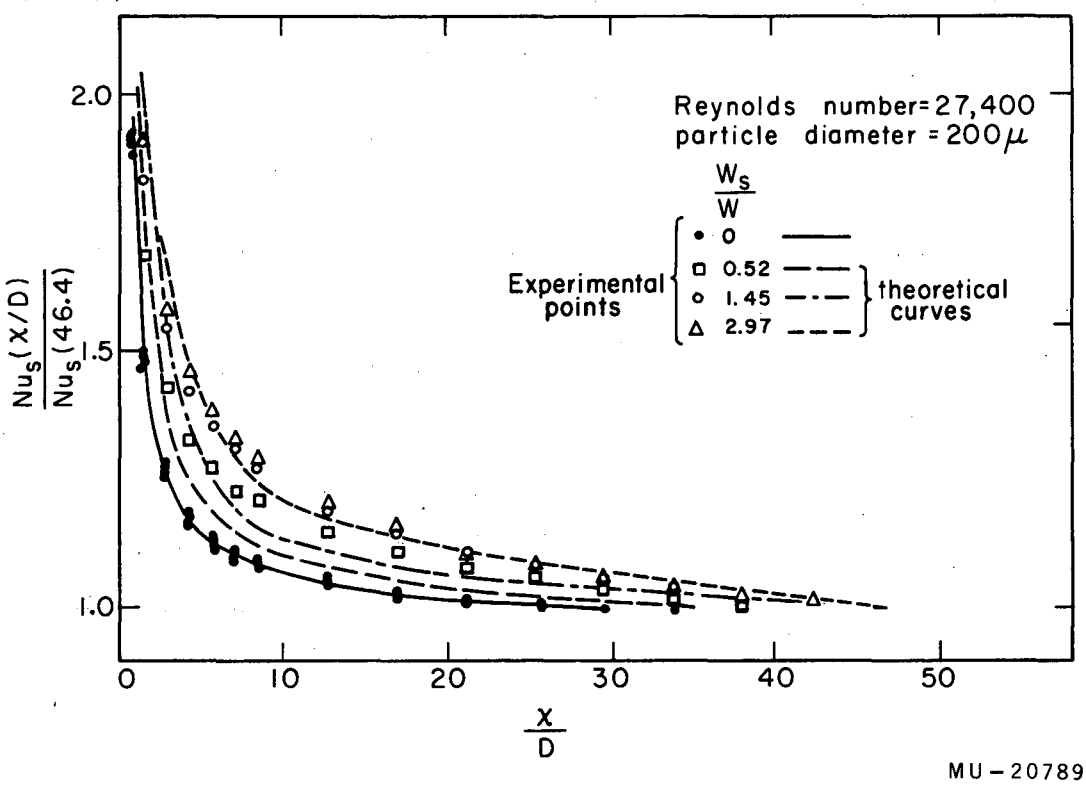

Fig. 16. Local Nusselt number ratio vs. axial distance at different loading ratios.

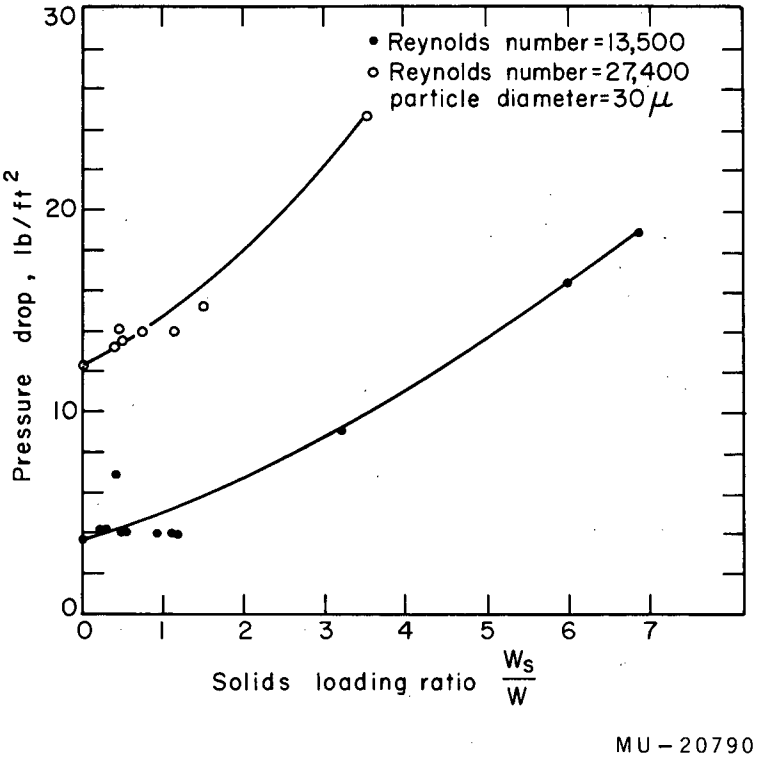

Fig. 17. Pressure drop vs. solids loading ratio.

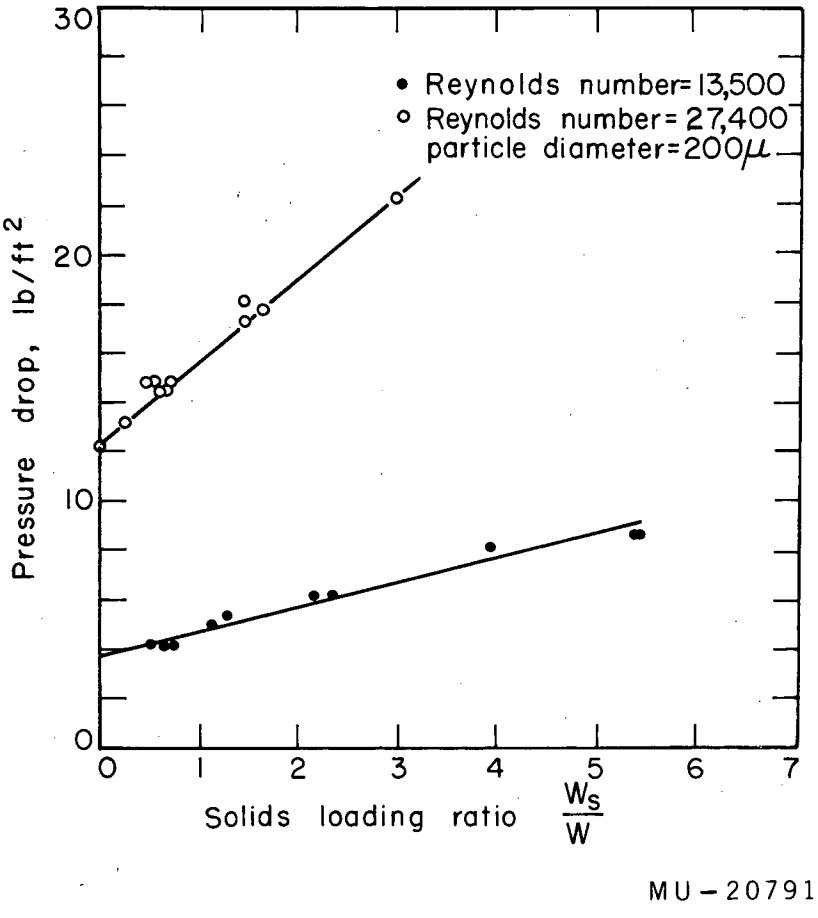

Fig. 18. Pressure drop vs. solids loading ratio.

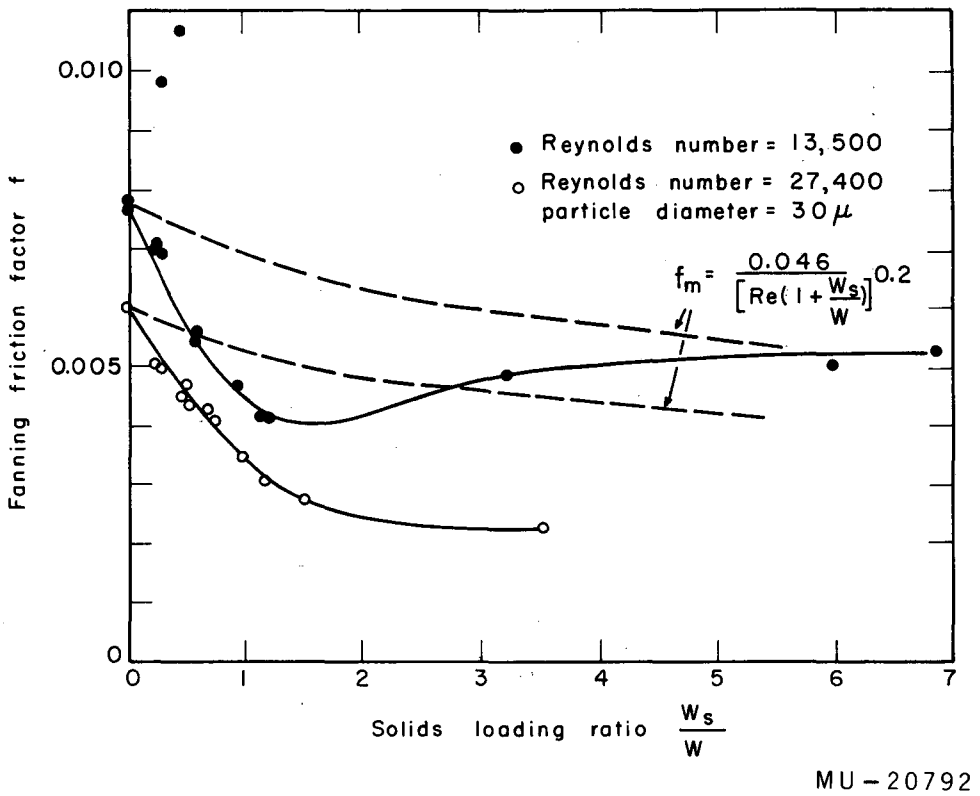

Fig. 19. Fanning friction factor vs. solids loading ratio.

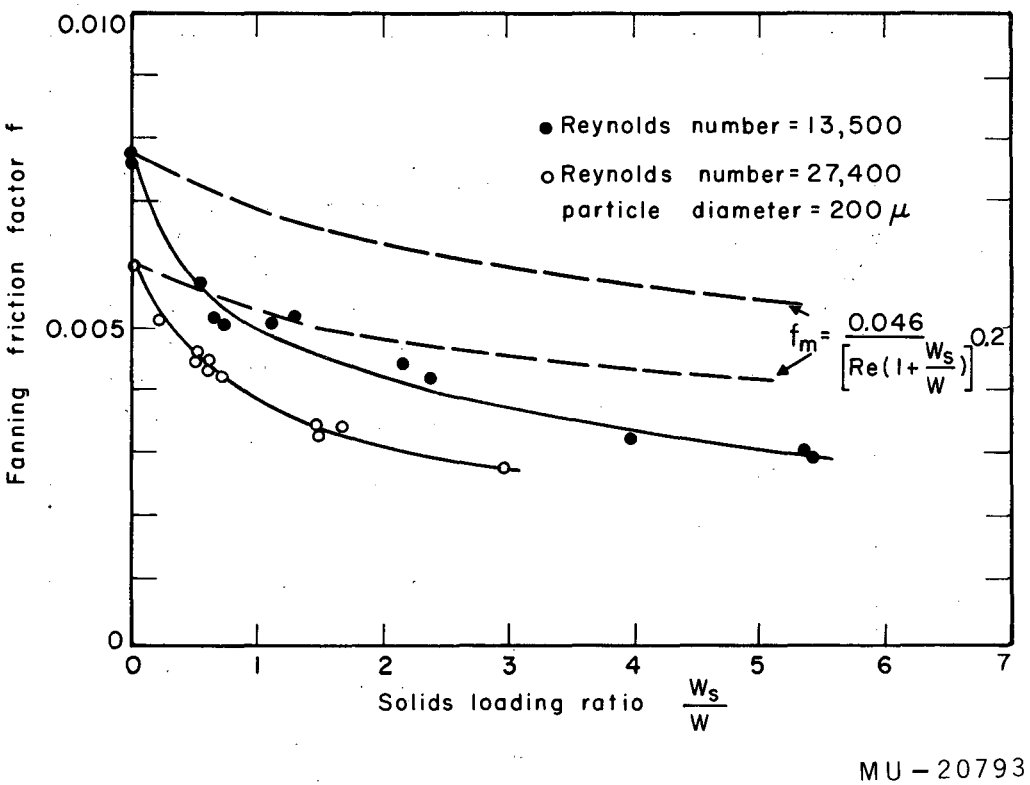

Fig. 20. Fanning friction factor vs. solids loading ratio.

The heat transfer section consisted of a 20-mm o.d. X 17-mm i.d. pyrex glass tube 31.75 inches long, heated with condensing carbon tetrachloride vapors. Heat-rate measurements were made by collecting condensate for timed periods.

Heat transfer coefficients were calculated on the basis of bulk mean air temperature at inlet and exit. The logarithmic mean temperature difference was arbitrarily used.

Results of the tests are shown in Fig. 21 in terms of the overall mixture heat transfer coefficients.

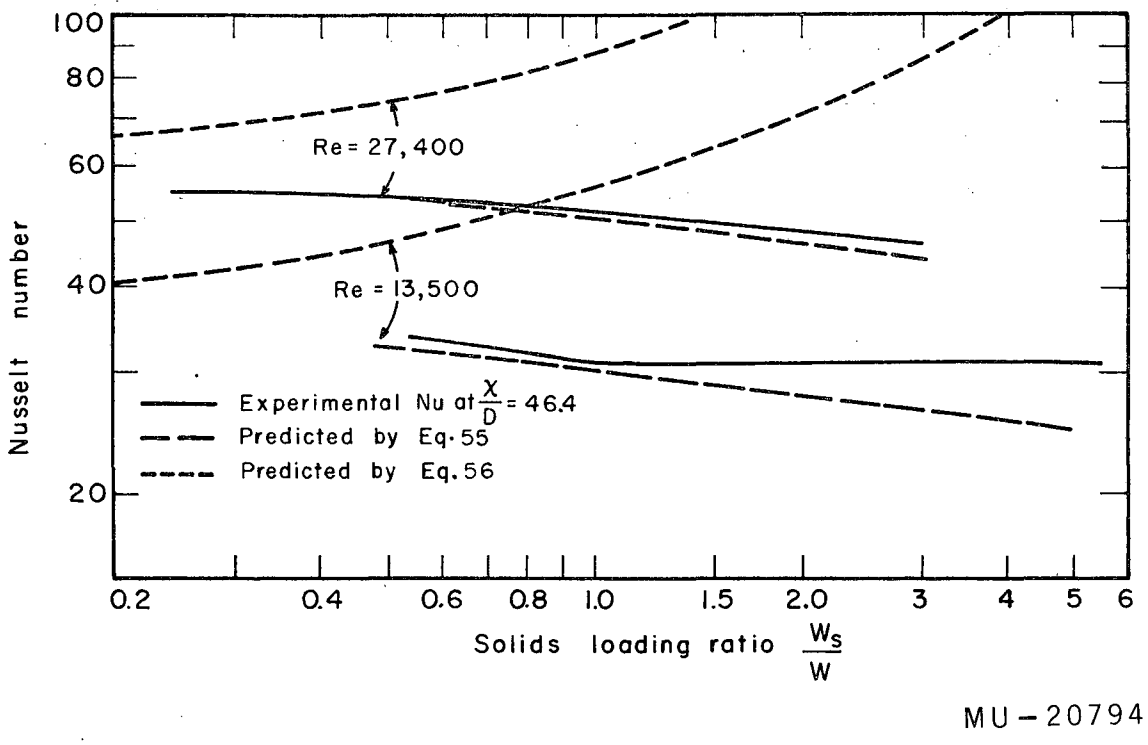

Fig. 21. Overall isothermal tube heat transfer coefficient vs. solids loading ratio, using 30 μ particles.

VI. DISCUSSION OF THE RESULTS

A. Heat Transfer with Air

The excellent agreement of the local Nusselt number variation–Fig. 5–w ith Sparrow's[18] result is noteworthy. The effect of Reynolds number on the 5% thermal entry length was found to be small over the range of air flow rates used. This is in quantitative agreement with the above analytical findings, where the entry length was from 12 to 14 pipe diameters over a range of Reynolds numbers from 50,000 to 100,000. Deissler's boundary layer model yields results that are quite different from the present findings which show considerably longer thermal entry regions. It is probable that the model does not accurately describe the physical situation in the region where the boundary layer thickness approaches the pipe radius.

The experimentally determined asymptotic Nusselt numbers are compared to the results of other investigators in Fig. 4. Excellent agreement is found with Sparrow's equation

$$Nu = 0.0245\ Re^{0.77}$$

for Pr = 0.7. Experimentally determined Nusselt numbers are within ±5% of this line. The results fall about 15% below the analytical findings of Sleicher and Tribus[14] and show better agreement with Deissler's[2] values. As a final comparison, the asymptotic Nusselt numbers are found to be about 10% below the Dittus-Boelter correlation for turbulent heat transfer in isothermal tubes. A recent note by Siegel and Sparrow[13] shows that Nusselt numbers for the isothermal wall boundary condition can be expected to be from 2.8 to 4.1% less than for the constant flux condition for air in the Reynolds number range from 10,000 to 50,000. This trend was not found in the present experimental results.

B. Pressure Drop with Air

Changes in a fluid velocity profile are manifested in varying local shear stress. Because the wall shear stress is balanced by pressure drop, the pressure gradient is a measure of changes in velocity distribution. Overall pressure drop measurements, converted to Fanning friction factors according to Appendix F, indicate that fully established flow prevailed throughout the heated section. Fig. 6, a plot of overall friction factors vs Reynolds numbers, shows the experimental results correlating to ±10% with the curve recommended by McAdams.[8] There was no discernable difference between the unheated-tube results and the heated-tube results.

Local pressure drop measurements (see Fig. 22) made in the drawn brass tube further substantiate the fully developed flow entrance condition at 20 pipe diameters downstream from the Venturi.

C. Heat Transfer with 30-micron Particles

Figure 11 displays the variation of Nusselt number with solids loading ratio at three pipe locations for the two constant air rates used in this study. The behaviour of the Nusselt number is quite different at low loading ratios than it is at high ratios. At loading ratios less than 0.5, the solids have no effect and the heat transfer coefficient remains constant at the value obtained with air alone. At higher loading ratios, the curves at all locations are parallel and the Nusselt number is proportional to $(W_s/W)^n(x/D)^m$. At the lower Reynolds number, $n = 0.54$ and $m = -0.28$, but at the higher Reynolds number, $n = 0.32$ and $m = -0.14$. Between these two regions of loading, the curves pass through a minimum. The minimum occurs for Re = 13,500 at $W_s/W = 1$ and for Re = 27,400 at $W_s/W = 1.5$. The divergence between the curves for 25.4 and 46.4 pipe diameters – showing that the heat transfer coefficient at these locations is no longer the same – is an indication of the increasing length of the thermal entry region. The decrease in the curve for $x/D = 46.4$ at the low air rate is considerable, and it is interesting to note that – at this minimum –

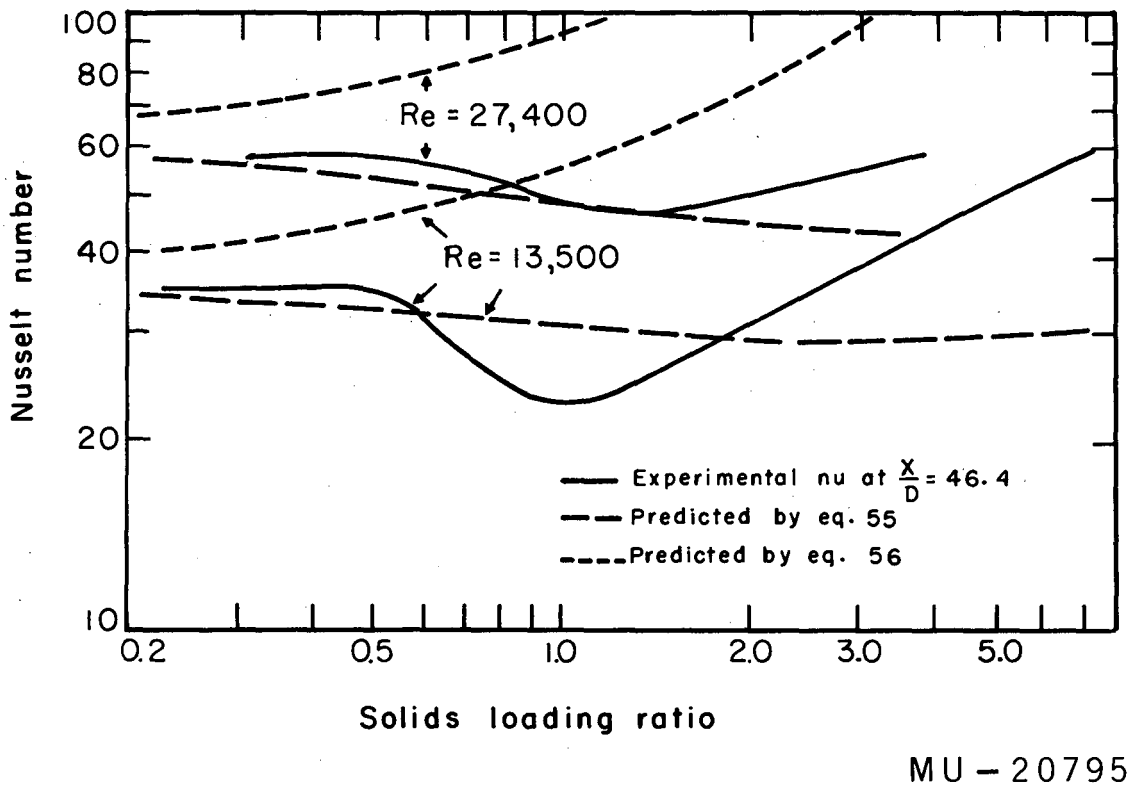

Fig. 22. Local pressure gradient in a brass tube.

the maximum heat transfer coefficient based on bulk mean air temperature that could exist is 14% below the value for air alone. With the exception of one run for Re = 13,500 and $W_s/W = 1.17$, the inlet temperature was constant within ±2%, and the tube wall temperature were constant within ±5%. Nevertheless, the heat flux decreases to a minimum at $W_s/W = 1$, which is 22% below the heat flux with air alone. Reference to Fig. 7 reveals the same variation, where for equal inlet wall temperatures a higher-placed curve indicates a lower heat flux. Notice in both Figs. 7 and 8 that the wall temperatures comes to a constant slope more quickly for high loading ratios than at lower concentrations. Although the curves are linear, they are not parallel to the line of two-phase mixture temperature, and they result in varying heat transfer coefficients.

The divergence of the curves for x/D = 25.4 and 46.4 in Fig. 11 gives rise to longer entry lengths. This result can be more easily seen in Figs. 13 and 14, which are curves of $Nu_s(46.4)$ plotted for only the lower loading ratios. The shape of the curves in unchanged at higher loading ratios; this is evident from the parallelism of the curves in Fig. 11.

D. Pressure Drop with 30-micron Particles

Overall pressure drop for the two-phase mixture is plotted as a function of solids loading in Fig. 17. Both curves exhibit a slight upward curvature. These measurements are converted to Fanning friction factors according to the equation derived in Appendix F. An initial assumption in the derivation was to assume that the solid phase was uniformly distributed, so that the flow could be treated as a homogeneous mixture. According to Fig. 19, friction factors calculated on this basis decrease as more solids are added. At the low air rate a minimum was observed, but at the higher air rate, the curve only approached a constant–but lower than with air alone–value. Compressor power limitations in the system did not allow the investigation to proceed to higher solids concentrations.

The curves show that the friction factor is lower than one would find from the correlation using the Reynolds numbers based on total mass

flow-DG_m/(viscosity of air). Because the friction factor is inversely proportional to Reynolds number, a decrease in the viscosity is indicated. There is some evidence to show that the viscosity is actually reduced by solids. Vanoni et al[22] have found in their experiments that the effect of sediment on the flow becomes appreciable even at moderate concentrations. To quote directly from their report, "It (the sediment) tends to reduce the so-called apparent, or eddy, viscosity which in turn tends to cause the velocity to increase." The results of this investigation support their views.

E. Heat Transfer with 200-micron Particles

The Nusselt numbers obtained with 200 μ beads are displayed in Fig. 12 in the manner used for the 30μ particles. Here the results are quite the same as above at the lower loading ratios-less than 0.5. A gradual decrease occurs beyond the 0.5 loading which continues for the higher air rate to the extent of the experimental range. For the lower air rate-Re = 13,500 - the curve stops decreasing, and the Nusselt number remains constant at a value that is about 10% lower than with air alone.

That the 200 μ particles were less effective than the 30 μ particles in cooling the wall is seen by comparing Figs. 9 and 10 with 7 and 8, which are curves of the dimensionless wall temperature vs. axial distance. These curves maintain a slight curvature for a considerable distance up the tube in contrast to the corresponding curves for the 30μ particles which quickly attained a constant slope.

Curves of the Nusselt number ratio $Nu_s/Nu_s(46.4)$ in Figs. 15 and 16 indicate an increasing thermal entry length with solids loading. For loading ratios greater than unity, however, the profiles are identical as shown by the superposition of the calculated points for the two highest ratios.

The wide variance in results between the heat transfer results for the two sizes has two possible explanations: (1) the surface to volume ratio is different by a factor of seven reducing the effective heat capacity for the large bead mixture; and (2) the pressence of a large number of

small particles – the ratio is 350:1 for equal loading ratios – may effect the spatial distribution due to the increased probability of particle-particle interaction.

F. Pressure Drop with 200-micron Particles

The curves of pressure drop vs. solids loading–Fig. 18–are linear. At the lower air rate, the slope is equal to the slope of the 30 μ particle curve at zero loading. At the higher air rate, the pressure drop with the two sizes is the same at a loading ratio of about 3. The variation of friction factor shown in Fig. 20 was about the same as was found with the smaller beads. One exception is that no minimum was produced at either air rate.

G. Heat Transfer in an Isothermal Tube with 30-micron Particles

The large increase in heat transfer coefficient produced by the presence of 30 μ particles is illustrated in Fig. 21 for two air Reynolds numbers–15,300 and 26,500. Results with 70μ and 200μ particles are reported in Reference 3. The coefficients are average with respect to area, and are based on the logarithmic mean difference between the tube wall temperature and the bulk-mean terminal air temperatures.

The coefficients can be expected to be higher in the isothermal tube than the coefficients at 46.4 pipe diameters in the constant heat flux tube for two reasons: (1) The mean air temperature is always greater than or equal to the bulk mean mixture temperature; (2) The isothermal tube coefficients are averages that include the thermal entry effects.

Comparing the results at the low Reynolds numbers it is found that a minimum occurs in the heat transfer coefficient at solids loadings of about unity for both of the above cases (Fig. 11 and 21). The coefficient decreases by about 10% from the value with air alone in the isothermal tube, but the value at 46.4 pipe diameters in Fig. 11 reaches a minimum that is 36% below the air alone value. The integrated average coefficient for uniform-wall flux is 20% below the air alone value.

Two reasons can be given for the difference in the amount of decrease for the two cases: (1) the air Reynolds numbers are different, and the results show that the decrease is less at higher air rates; and (2) the difference between the bulk mean air and mixture temperatures would make the isothermal tube results higher.

At higher loading ratios the two cases are comparable, but the isothermal tube coefficients have increased more–in comparison with the air alone value–than for the constant heat flux case, e.g., at $W_s/W = 7$ the coefficient for constant tube temperature has increased by 2-1/2, but the average constant heat flux value has increased only by 2. One would expect the difference in the definitions of h to be more important at high solids concentrations, and this is probably the main reason for the lack of quantitative agreement.

The results at the higher air rates compare well as can be seen by referring again to Figs. 11 and 21. In both cases, the increase begins at higher loadings than before. The minimum is not detectable within the scatter of the data in Fig. 11 and the decrease is only slight in Fig. 21.

Experimental results for both systems with 200 μ beads are in good quantitative agreement. The heat transfer coefficient decreased for loadings less than unity and remained at a constant value about 10% below the air alone coefficient.

Explanations can be offered for the behavior of the isothermal tube system by observing the local results in the present system. Increases in heat transfer are due to the longer thermal entry region. When a decrease occurs, all of the local values decrease accordingly. It is unfortunate that asymptotic performance at high loadings could not be measured, but one can conclude that a loading ratios greater than 1, the isothermal tube was shorter than the thermal entry region.

H. Comparison of Heat Transfer Results with the Theoretical Analysis

The theoretical analysis presented in Appendix D is divided into two parts: (1) theory derived from the energy equation, and (2) analogy between heat transfer and fluid friction. The model for which an approximate solution is obtained has a uniform distribution of solids and a velocity distribution that is unaffected by solids. This model is only one of many that could be proposed; it could be assumed that the solids are concentrated in the central region of the pipe or at the wall and that the velocity distribution is affected in a certain way. Because no investigator has successfully predicted the radial distribution of particles or the effect on the continuous phase velocity, it was decided to investigate the simplest possible case, and to compare the results with experimental measurements.

The theoretical analysis which is developed in Appendix D, Part A, produces the following expression for the local Nusselt number:

$$Nu_s = \frac{1}{1/Nu(X^+) + \frac{1}{2}(\theta_m - \theta_{mm})_\infty}$$

where $X^+ = \dfrac{x^+}{(1 + \frac{W_s}{W})}$ denotes that the Nusselt number for air alone is evaluated at X^+. $(\theta_m - \theta_{mm})_\infty$, has been found to be approximately equal to

$$\frac{W_s c_s}{(W_s c_s + W c)^2} \quad \frac{2\pi k U_m}{K_2}$$

The first factor is zero for both zero and very high loading ratios, and it reaches a maximum at $W_s c_s = W c \left(\frac{W_s}{W} = 1.26\right)$. The second factor is a constant for a particular particle size and gas Reynolds number. Considering only changes in the solids loading, the first term in the denominator of the equation for Nu_s decreases with increasing solids loading $Nu_s(X^+)$ increases with decreasing X^+. The second term, $(\theta_m - \theta_{mm})_\infty$, increases to a maximum and then decreases.

The net effect is that Nu decreases to a minimum in the region $0.5 < W_s/W < 1.5$. and then increases (An exception to this rule occurs for 30 μ beads at less than 8.4 pipe diameters). This effect is largest with 200μ beads where the Nusselt number reaches a minimum 18% below the value without solids.

Figures 11 and 12 show that the agreement of the analysis with the experimental results is only qualitative. The decrease in Nu_s for the 30μ beads is much more than the theory predicts. One might say that the approximation for $(\theta_m - \theta_{mm})_\infty$ is the reason for this inconsistency, if it were not for the fact that when the theory predicts a more significant decrease (for 200 μ beads) due to $(\theta_m - \theta_{mm})_\infty$, the change is experimentally found to be less.

The analyis qualitatively agrees with the data in Fig. 12 for 200μ spheres up to loading ratios of about unity, but the predicted rise in Nu_s was not found experimentally. This increase is largely due to the fact that $(\theta_m - \theta_{mm})_\infty$ is proportional to $W_s c_s/(W_s c_s + W c)^2$ which approaches zero at high loading rates. Previous experimental work in Reference 3 shows that the difference between bulk gas and solids temperatures at the outlet of an isothermal tube is constant with solids loading. If this is approximately true in the present system, $(\theta_m - \theta_{mm})_\infty$ is proportional to $W_s c_s/(W_s c_s + W c)$ which is zero for no solids and approaches unity at high rates. This dependency is in better agreement with the data than is the approximation made in Appendix D. This increased significance of $(\theta_m - \theta_{mm})_\infty$ at high loadings would not effect the predictions for the 30μ beads since the term is always small for the smaller size. As previously discussed in the section Heat Transfer with 30-micron Particles, the addition of solids decreased the heat flux for the same wall temperature. This result is not qualitatively predicted by the analysis – indicating that the model does not adequately describe the system.

Figures 13, 14, 15, and 16 compare the theoretically predicted ratio of the local Nusselt number to Nusselt number at 46.4 pipe diameters with the experimental results. Although the curves show fair agreement, the comparison is somewhat misleading. Experimentally, the higher local ratio is due to the decrease in the denominator and not–as theory predicts–due to higher local coefficients. The curves plainly point out the longer thermal entry region as solids are added.

Several of the initial assumptions are open to criticism. As previously mentioned–the assumption that particles are everywhere evenly distributed is a pure supposition. It may be argued that the population should be greater either in the vicinity of the wall or within the central turbulent core. One can admit with equal probability the force described by Soo and Tien[17] due to a spinning motion of the spheres in a sharp mean velocity gradient which would move the particles to the center or a centrifugal force due to a circular motion about the axis which would move the particles to the wall.

Assumption 4 of Appendix D–no effect of solids on continuous phase velocity–is no more justified than the one that is discussed above. Hans Meyer's[9] measurements show a considerable deviation from the 1/7th power law at a solids loading of only 0.4. If a non-uniform distribution of solids is admitted, certainly the velocity profile will be affected. The change could be either towards a more plug like profile or a more streamline profile.

The criticisms offered in the preceding paragraphs against the theory derived from the energy equation lead one to make other attempts to predict the effects on heat transfer. Because wall shear stress measurements were available, the analogy between fluid friction and heat transfer was used in Appendix D, Part B, to gain better agreement than had been produced in Part A. In the derivation from the energy equation, it was necessary to use of values of r_0^+ from the clear-gas flow. The pressure drop measurements yield values of wall shear stress, τ_0, but the problem arises as to how to evaluate the properties involved in r_0^+, namely ρ, and ν. It is logical to consider the density as being the total density ρ_s, but the basis for ν is less clear. Figures 23 and 24 show the results obtained from Eq.(55) when ν is unchanged and the prediction from Eq. (56) when ν is evaluated for total density. Because the analogy predicts values for the asymptotic performance, the theoretical curves should fall below the experimentally determined curve. The curve from Eq. (56) is so far from the experimental result that the idea of changing ν for the density is untenable.

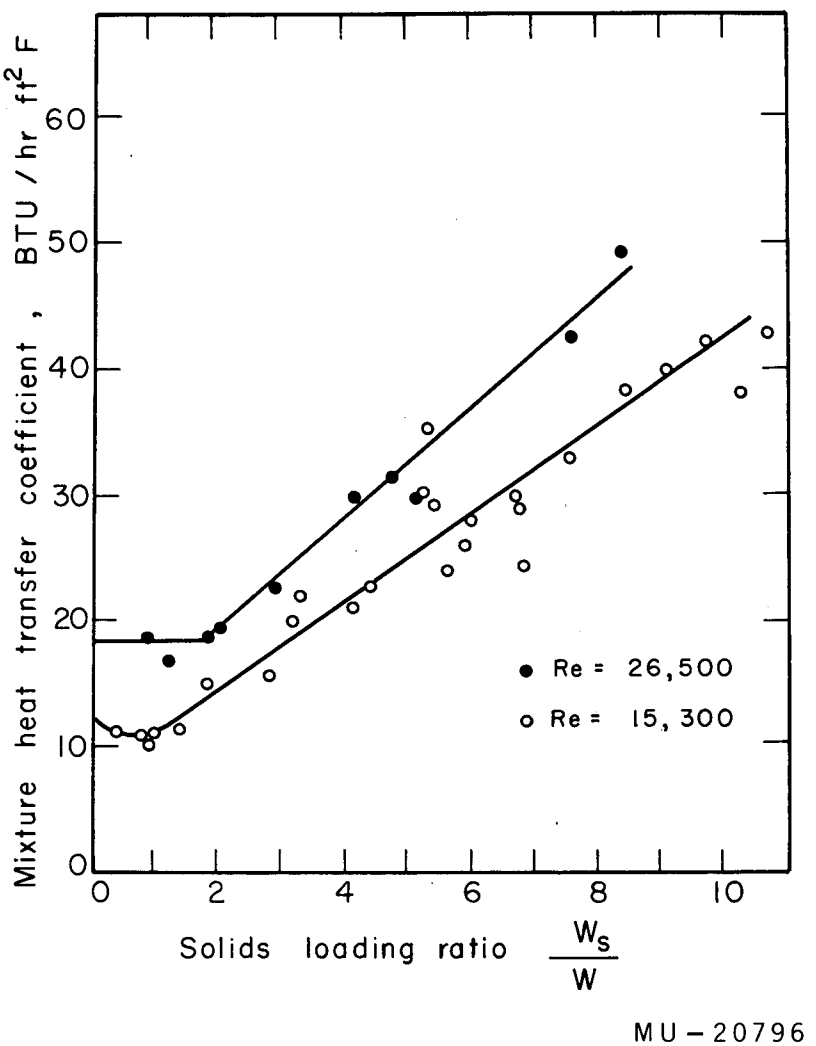

Fig. 23. Nusselt number vs. solids loading ratio, using 30 μ particles.

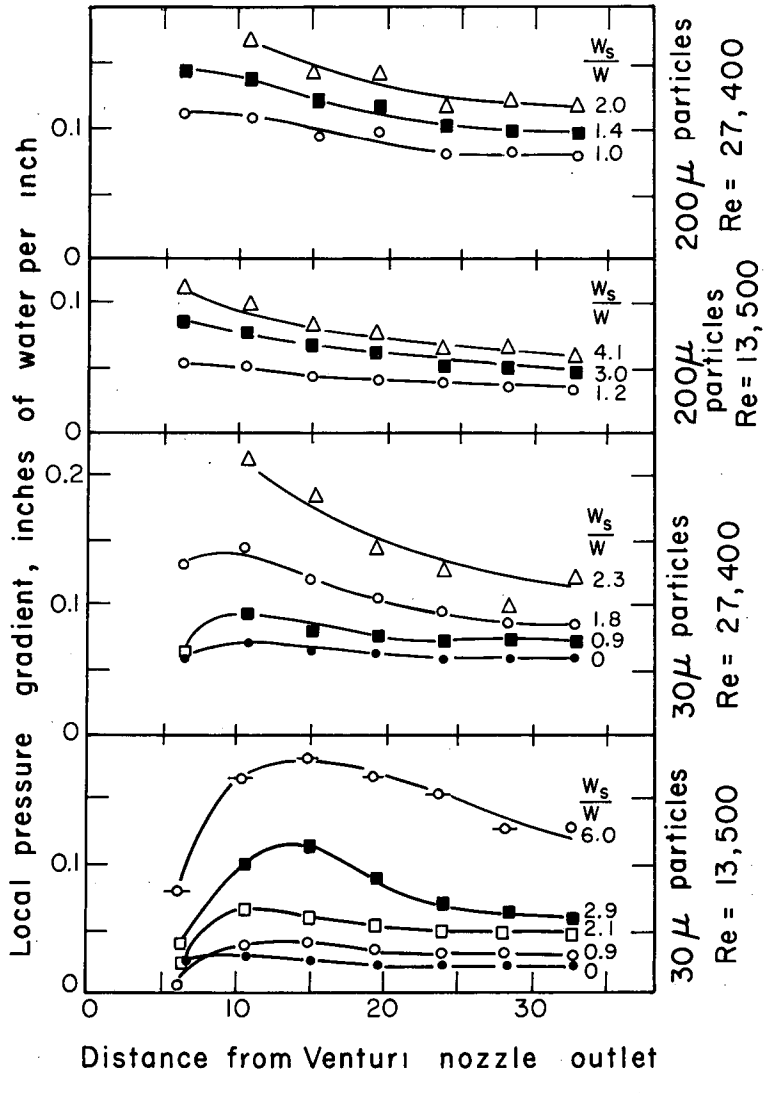

Fig. 24. Nusselt number vs. solids loading ratio, using 200 μ particles.

One might say that the correct theory lies somewhere between the two curves if it were not for the behaviour of the experimental result for 30μ at Re= 13,500. It is clear that the transport properties have been greatly reduced in the region of unity solids loading and that the concept of a homogenous mixture is far from the truth.

The analogy is in fair agreement with the results for the 200 μ beads as shown in Fig. 24, but is is clear from a comparison of the results for the two particle sizes that the theory for the solution of the hydrodynamic problem will have to be quite extensive.

I. Recommendations for Further Study

1. Further analytical and experimental work on the effect of the solid phase on the continuous phase motion should be done.

2. Experiments using a constant heat flux tube of considerably longer length than the present one would yield valuable information regarding the length of the thermal entry region.

3. A better approximation to the difference between the bulk gas and solids temperatures would improve the present analysis.

VII. CONCLUSIONS

The following statements pertain to a system having solid spherical glass particles entrained in an air stream with a fully developed velocity profile at the inlet to a heated tube having a uniform heat flux.

It may be concluded from the results of this investigation that:

1. The theoretical model, which assumes that the air and solids act as a homogeneous mixture with nearly equal local temperatures and the same velocity distribution as the unladen air, is inadequate to describe the heat transfer effects in a flowing gas-solids mixture as indicated in Figs. 11 and 12.
2. At solids loading ratios less than 0.5, there is practically no effect on the heat transfer rate and coefficient at the tube wall.
3. The local Nusselt number, as defined in this dissertation, is essentially unaffected by 200 μ particles up to loading ratios of to 7.
4. The distance from the inlet to the point where a fully established temperature profile persists is increased by the addition of 30 μ particles.
5. At solids loadings greater than 1.5 with 30 μ particles, the local Nusselt numbers at pipe locations less than 46.4 pipe diameters, increase proportional to $(W_s/W)^n$. $n = 0.54$ for $Re = 13{,}500$, and $n = 0.32$ for $Re = 27{,}400$.
6. Pressure drop for solids loadings less than 7 is less than would be expected on the basis of increased mass of a homogeneous mixture.

VIII. NOMENCLATURE

A_p = surface area of particle, ft^2

a = radius of a particle, ft

B_n^2 = constant defined by Eq. (28)

C = constant defined by Eq. (27)

C_s = constant defined by Eq. (27)

c = heat capacity of air, BTU/lb F

c_s = heat capacity of solids, BTU/lb F

D = duct diameter, ft

f = Fanning friction factor

G = mass velocity of air, $lb/hr\ ft^2$

G_m = mixture mass velocity, $lb/hr\ ft^2$

H_1 = defined by Eq. (16)

H_2 = defined by Eq. (17)

h = pipe wall heat transfer coefficient, defined by Eq. (39a), $BTU/hr\ ft^2\ F$

h_p = particle surface heat transfer coefficient, $BTU/hr\ ft^2\ F$

K_1 = $n_p \frac{Nu_p}{2a} A_p$, hr^{-1}

K_2 = $\frac{Nu_p\ k\ A_p}{2\ \rho_p\ C_s\ V_p\ a}$, hr^{-1}

k = air thermal conductivity, BTU/hr ft F

L = duct length, ft

Nu = Nusselt number with air

Nu_s = Nusselt number with air and solids

Nu_p = particle Nusselt number

n_p = number of particles per unit volume, ft^{-3}

P = air pressure, lb/ft^2

Pe_m = mixture Peclet number, $RePr(1 + \frac{W_s C_s}{WC})$

P_r = Prandtl number, $\frac{\nu}{a}$

q = tube wall heat flux, $BTU/hr\ ft^2$

R = gas constant, ft / ^{o}R

Re = Reynolds number = $\frac{U_m D \rho}{u}$

Re_s = Reynolds number = $\frac{U_m D \rho_s}{u}$

Re_p = particle Reynolds number based on relative velocity

r = radial distance, ft

r^+ = dimensionless radius, $\frac{r\sqrt{\frac{\tau}{\rho}}}{\nu}$

T = air temperature, ^{o}R

T_{av} = two-phase mixture average terminal temperature, ^{o}R

T_1 = inlet mixture temperature, ^{o}R

T_2 = outlet mixture temperature, ^{o}R

T_s = solids temperature, R

u = axial velocity, ft/hr

u_m = bulk mean axial gas velocity, ft/hr

u^+ = dimensionless velocity $u/\sqrt{\tau_0/\rho}$

V_s = volume of a particle, ft^3

W = weight flow rate of air, lb/hr

W_s = weight flow rate of solids, lb/hr

x = axial distance, ft

x^+ = dimensionless axial distance, $\frac{x}{r_0}$

α = gas thermal diffusivity, ft^2/hr

βn^2 = eigenvalues of Eq. (35)

Γ = $K_1 \frac{\nu r_0^+}{\tau_0/\rho}$

γ = dimensionless thermal diffusivity, $\frac{\alpha+\epsilon_H}{\nu}$

ϵ_H = eddy diffusivity for heat

ϵ_m = eddy diffusivity for momentum

θ = dimensionless temperature

θ_s = dimensionless particle temperature

ν = kinematic viscosity, lb/hr ft

χ = defined by Eq. (27)

ψ = defined by Eq. (27)

ψ_s = dimensionless temperature

ρ = gas density, lb/ft^2

ρ_s = solids density, lb/ft^3

τ_0 = wall shear stress, lb/ft^2

$\Omega = K_2 \frac{\nu r_0^+}{\tau_0/\rho}$

θ_m = bulk mean air temperature

θ_{ms} = bulk mean solids temperature

θ_{mm} = bulk mean mixture temperature

Subscripts

0 = wall conditions

1 = inlet conditions

2 = exit conditions

p = pertaining to a discreet particle

s = pertaining to the solid phase

∞ = evaluated far down the pipe

Table I

Reynolds No.	Net heat flux BTU/hr ft^2	Inlet temp. ^oF	$T_m @ \frac{x}{D} = 46.4$ ^oF	$T_0 @ \frac{x}{D} = 46.4$ ^oF	h_∞ BTU/hr ft^2 F
11,400	980	75.7	155.3	273.0	8.4
13,500	1190	74.3	162.2	276.2	10.35
13,500	1190	74.0	161.9	274.6	10.5
13,500	1139	75.7	159.6	270.3	10.2
13,500	1200	70.7	159.2	269.6	10.6
13,500	1121	73.7	156.2	266.7	10.1
13,700	1220	69.0	158.9	276.3	10.3
15,500	1730	76.0	181.3	342.0	10.8
15,800	1262	75.7	150.7	267.4	10.9
18,700	2035	75.7	178.7	338.6	12.8
19,400	1545	77.0	152.5	273.5	12.9
23,000	2410	76.0	176.7	340.0	14.9
23,600	1720	75.7	147.3	264.1	14.9
24,000	1815	71.0	146.9	265.5	15.3
27,000	2020	76.3	150.7	269.6	17.2
27,000	2020	74.7	149.1	270.3	16.8
27,300	2010	71.3	145.3	266.7	16.5
27,400	2045	75.3	149.4	274.0	16.5
28,500	2075	76.0	147.6	268.7	17.3
28,800	2900	75.7	174.0	339.9	17.6
33,600	3480	71.0	169.4	339.3	20.5
33,800	2520	70.7	141.3	267.0	20.2
41,100	4030	73.7	167.1	336.3	23.8
41,400	2960	70.3	138.0	263.7	23.6

Table II

Local values of $h(x/D) / h_\infty$ for air

Reynolds No.	Local $h(x/D) / h_\infty$ at x/D															
	0.704	1.41	2.82	4.23	5.64	7.04	8.44	12.6	16.0	21.1	25.4	29.6	33.8	38.0	42.3	46.4
11,400	2.27	1.65	1.34	1.22	1.16	1.13	1.10	1.05	1.03	1.01	1.01	1.00	1.00	1.00	1.00	1.00
13,500	2.08	1.54	1.27	1.16	1.11	1.07	1.05	1.03	1.02	1.00	1.00	1.00	1.00	1.00	1.01	1.00
13,500	2.03	1.51	1.24	1.13	1.08	1.05	1.04	1.03	1.01	1.01	1.01	1.00	1.00	1.00	1.00	1.00
13,500	2.15	1.60	1.29	1.18	1.13	1.10	1.08	1.04	1.03	1.01	1.01	1.01	1.00	1.00	1.00	1.00
13,500	2.02	1.51	1.25	1.15	1.10	1.07	1.05	1.02	1.01	1.00	1.00	1.00	1.00	1.01	1.02	1.00
13,500	2.10	1.56	1.29	1.18	1.13	1.09	1.07	1.03	1.01	1.00	1.00	1.00	1.00	.99	1.00	1.00
13,700	2.07	1.55	1.26	1.16	1.12	1.08	1.06	1.03	1.01	1.00	1.00	1.00	1.00	1.00	1.00	1.00
15,500	2.17	1.60	1.32	1.21	1.16	1.12	1.10	1.05	1.03	1.01	1.01	1.00	1.00	1.00	1.00	1.00
15,800	2.13	1.58	1.30	1.20	1.15	1.12	1.10	1.05	1.03	1.02	1.01	1.00	1.00	1.00	1.00	1.00
18,700	2.06	1.55	1.29	1.20	1.15	1.11	1.09	1.05	1.02	1.01	1.00	1.00	1.00	1.00	1.00	1.00
19,400	2.06	1.55	1.30	1.20	1.15	1.11	1.09	1.05	1.03	1.02	1.01	1.00	1.00	1.00	1.00	1.00
23,000	2.00	1.52	1.28	1.19	1.15	1.11	1.09	1.05	1.03	1.01	1.01	1.00	1.00	1.00	1.00	1.00
23,600	2.02	1.53	1.29	1.20	1.15	1.11	1.08	1.06	1.02	1.01	1.00	1.01	.99	1.00	1.00	1.00
24,000	1.92	1.48	1.26	1.17	1.12	1.09	1.07	1.03	1.02	1.01	1.00	1.00	1.00	1.00	.99	1.00
27,000	1.91	1.48	1.25	1.16	1.12	1.09	1.08	1.05	1.03	1.01	1.01	1.00	.99	1.00	1.00	1.00
27,000	1.88	1.46	1.25	1.16	1.12	1.08	1.08	1.05	1.03	1.02	1.01	1.00	1.00	1.00	1.00	1.00
27,300	1.91	1.49	1.28	1.19	1.14	1.11	1.09	1.06	1.04	1.02	1.01	1.01	1.00	1.00	1.00	1.00
27,400	1.90	1.49	1.27	1.18	1.13	1.11	1.09	1.05	1.03	1.02	1.01	1.01	1.00	1.00	1.00	1.00
28,500	1.94	1.49	1.27	1.18	1.14	1.11	1.09	1.05	1.03	1.01	1.00	1.00	.99	1.00	1.00	1.00
28,800	1.93	1.49	1.28	1.18	1.14	1.11	1.09	1.04	1.03	1.01	1.00	1.00	1.00	1.00	.99	1.00
33,600	1.81	1.44	1.25	1.18	1.14	1.11	1.08	1.04	1.02	1.01	1.01	1.00	1.00	1.00	1.00	1.00
33,800	1.79	1.44	1.25	1.17	1.13	1.10	1.09	1.06	1.03	1.02	1.01	1.01	1.00	1.00	1.00	1.00
41,100	1.76	1.42	1.25	1.18	1.14	1.11	1.09	1.05	1.03	1.01	1.00	1.00	1.00	1.00	1.00	1.00
41,400	1.77	1.43	1.25	1.18	1.14	1.11	1.09	1.06	1.03	1.03	1.02	1.01	1.01	1.00	1.00	1.00

Table III

Heated tube friction factor with air

Reynolds No.	$G \times 10^{-4}$ lb/hr ft^2	Inlet pressure $\times 10^{-3}$ psfa	Pressure drop psf	T_{av} ^{o}R	f
13,500	1.05	2.08	3.7	581.9	.00773
13,500	1.05	2.08	3.7	581.6	.00773
13,500	1.05	2.08	3.7	581.1	.00777
13,500	1.05	2.08	3.7	578.6	.00785
13,500	1.05	2.07	4.1	578.4	.00688
13,700	1.05	2.07	8.6	552.2	.00867
15,500	1.22	2.07	4.9	593.1	.00715
15,800	1.25	2.07	6.6	576.3	.00750
18,700	1.46	2.05	7.4	591.5	.00755
19,400	1.50	2.05	6.6	577.8	.00670
23,000	1.80	2.03	9.9	590.6	.00639
23,600	1.83	2.03	9.1	574.4	.00611
27,000	2.10	2.03	11.5	576.5	.00574
27,000	2.10	2.02	12.4	574.9	.00604
27,300	2.10	1.99	11.9	571.3	.00588
27,400	2.14	2.00	12.4	575.4	.00582
28,500	2.21	2.00	12.4	575.7	.00552
28,800	2.26	1.99	14.0	589.0	.00550
41,100	3.34	1.89	28.2	584.4	.00466
41,400	3.37	1.89	28.2	567.9	.00500

Table IV

$\theta_2(x^+, r_0^+)$ for air in heated and adiabatic sections

	θ_2 at $\frac{x}{D}$ for various Reynolds Nos.												
x/D	11,400	15,500	15,800	18,700	19,400	23,000	23,600	28,500	28,800	33,600	33,800	41,100	41,400
(Heated section)													
0.70	36.0	27.0	26.2	24.0	21.5	36.5	18.3	15.1	14.8	11.8	11.8	9.8	10.0
1.41	25.4	18.8	18.2	16.5	14.9	12.5	12.6	10.2	10.1	8.1	8.1	6.7	7.0
2.11	16.3	12.1	11.5	10.4	9.6	8.0	8.1	6.7	6.6	5.3	5.3	4.5	4.6
2.82	11.6	8.7	9.6	7.5	6.8	5.9	5.9	4.8	4.7	3.9	3.9	3.5	3.5
4.23	8.9	6.9	6.5	5.9	5.4	4.7	4.7	3.8	3.8	3.2	3.0	2.8	2.8
5.64	7.2	5.4	5.1	4.6	4.2	3.5	3.5	3.1	3.1	2.5	2.5	2.2	2.3
7.04	5.9	4.6	4.3	3.9	3.5	3.1	3.0	2.5	2.5	2.0	2.3	1.9	2.0
8.44	3.1	2.1	2.4	2.2	2.1	1.7	2.0	1.5	1.2	1.1	1.5	1.04	1.2
12.58	1.9	1.4	1.6	1.2	1.3	0.94	0.82	0.91	0.81	0.59	0.86	0.56	0.75
16.88	0.82	0.69	0.83	0.59	0.66	0.4	0.36	0.31	0.39	0.31	0.45	0.27	0.56
21.13	0.51	0.25	0.49	0.21	0.33	0.18	0	0.09	0.31	0.13	0.27	0	0.34
(Adiabatic section)													
0.70	7.0	5.8	5.7	5.6	5.3	1.2	4.7	4.2	4.6	4.4	6.3	2.8	4.8
1.41	4.8	3.8	3.8	3.4	3.5	0.7	3.0	2.7	2.7	2.5	2.7	2.3	2.3
2.11	2.4	1.9	1.9	1.8	1.7	0.34	1.5	1.3	1.4	1.3	1.4	1.2	1.1
2.82	1.1	0.82	0.77	0.81	0.81	0.14	0.7	0.66	0.6	0.6	0.67	0.46	0.51
4.23	0.44	0.19	0.26	0.26	0.25	0.04	0.22	0.21	0.19	0.23	0.22	0.22	0.24
5.64	0.11	0.19	0	0.03	0	0.03	0	0	0	0	0	0	0

Table V

Two-phase heat transfer [a]

W_s / W	Net heat flux BTU/hr ft^2	Inlet temp. ^oF	T_{mm} @ ^oF $\frac{x}{D} = 46.4$	T_0 @ ^oF $\frac{x}{D} = 46.4$	h(46.4) BTU/hr ft^2 F
(Re = 13,500; W = 29.0 lb/hr)					
0.247	1193	73.0	146.5	267.7	9.9
0.265	1193	72.3	144.7	265.0	9.9
0.266	1193	70.7	143.0	264.1	9.85
0.272	1193	70.0	142.1	265.8	9.7
0.429	1250	68.7	136.0	265.8	9.65
0.57	1250	72.0	137.7	274.0	9.05
0.58	1180	71.7	131.1	263.5	8.9
0.78	1250	69.3	128.1	303.0	7.15
0.95	936	72.3	114.0	260.5	6.4
1.15	1042	72.7	112.7	271.3	6.6
1.17	1042	73.7	113.4	272.3	6.6
3.2	1700	74.7	104.3	269.7	10.3
5.96	2150	89.7	117.9	267.0	14.4
6.85	2300	86.7	112.8	271.3	14.5
(Re = 27,400; W = 59.0 lb/hr)					
0.45	2020	77.0	131.4	262.8	15.5
0.51	2080	76.7	131.0	268.7	15.7
0.74	2080	76.7	116.8	265.1	14.0
1.14	2160	76.3	117.8	269.4	14.3
1.50	2145	80.3	116.3	273.0	13.7
3.50	2690	77.0	103.2	271.3	16.0

[a] Particle size = 30 μ

Table VI

Local values of h(x/D)/ h(46.4)[a]

W_s/W	h(46.4) BTU/hr ft^2 F	Local h(x/D) / h(46.4) at x/D															
		0.704	1.41	2.82	4.23	5.64	7.04	8.44	12.6	16.9	21.1	25.4	29.6	33.8	38.0	42.3	46.4
(Re = 13,500; W = 29 lb/hr)																	
0.247	9.9	2.24	1.65	1.34	1.215	1.15	1.12	1.09	1.06	1.035	1.01	1.007	1.002	0.995	1.00	1.00	1.00
0.265	9.9	2.28	1.66	1.35	1.22	1.14	1.12	1.10	1.06	1.03	1.01	1.00	1.00	0.995	0.995	1.00	1.00
0.266	9.85	2.24	1.66	1.35	1.235	1.17	1.13	1.10	1.06	1.04	1.015	1.007	1.00	0.995	0.995	1.00	1.00
0.272	9.7	2.28	1.69	1.37	1.25	1.17	1.14	1.11	1.065	1.04	1.02	1.005	1.005	1.00	1.00	1.002	1.00
0.429	9.65	2.22	1.70	1.38	1.26	1.18	1.14	1.115	1.07	1.04	1.015	1.01	1.006	1.00	1.00	1.002	1.00
0.57	9.05	2.44	1.81	1.46	1.32	1.238	1.182	1.145	1.072	1.033	1.01	1.00	1.00	1.00	1.002	1.01	1.00
0.58	8.9	2.42	1.79	1.438	1.303	1.22	1.17	1.135	1.073	1.03	1.01	1.003	0.996	0.996	0.996	1.00	1.00
0.78	7.15	3.08	2.22	1.77	1.59	1.47	1.41	1.36	1.25	1.16	1.11	1.08	1.04	1.02	1.025	1.005	1.00
0.95	6.4	3.18	2.40	1.935	1.73	1.61	1.54	1.47	1.325	1.248	1.178	1.127	1.082	1.05	1.03	1.013	1.00
1.15	6.6	3.40	2.52	2.03	1.83	1.74	1.635	1.56	1.415	1.32	1.248	1.18	1.13	1.082	1.043	1.02	1.00
1.17	6.6	3.40	2.53	2.04	1.828	1.703	1.635	1.56	1.415	1.32	1.24	1.175	1.13.	1.082	1.043	1.02	1.00
3.20	10.3	3.21	2.49	2.20	2.04	1.94	1.87	1.80	1.63	1.49	1.40	1.31	1.23	1.17	1.10	1.056	1.00
5.96	14.4	2.78	2.14	1.89	1.76	1.67	1.63	1.61	1.50	1.415	1.348	1.275	1.21	1.15	1.093	1.055	1.00
6.85	14.5	2.68	2.13	1.92	1.78	1.72	1.69	1.66	1.545	1.45	1.37	1.295	1.225	1.155	1.09	1.046	1.00
(Re = 27,400; W = 59 lb/hr)																	
0.45	15.5	2.06	1.612	1.36	1.26	1.212	1.18	1.148	1.109	1.073	1.043	1.031	1.022	1.011	1.006	1.006	1.00
0.51	15.7	2.08	1.605	1.37	1.27	1.218	1.18	1.17	1.115	1.076	1.05	1.038	1.022	1.011	1.005	1.003	1.00
0.74	14.0	2.44	1.73	1.458	1.342	1.287	1.242	1.23	1.165	1.12	1.082	1.063	1.05	1.028	1.013	1.013	1.00
1.14	14.3	2.24	1.69	1.41	1.30	1.245	1.218	1.19	1.115	1.09	1.062	1.042	1.027	1.018	1.008	1.008	1.00
1.50	13.7	2.60	1.795	1.48	1.363	1.307	1.262	1.218	1.16	1.125	1.088	1.072	1.05	1.037	1.013	1.01	1.00
3.50	16.0	2.39	1.81	1.56	1.46	1.405	1.345	1.315	1.24	1.19	1.145	1.118	1.09	1.068	1.035	1.02	1.00

[a]Bead size = 30 μ.

Table VII

Two-phase heat transfer[a]

W_s/W	Net heat flux BTU/hr ft^2	Inlet temp ^oF	T_{mm} @ ^oF x/D = 46.4	T_w @ ^oF x/D = 46.4	h(46.4) BTU/hr ft^2 F
(Re = 13,500; W = 29.0 lb/hr)					
0.524	1222	73.3	136.8	269.7	9.29
0.666	1250	71.0	131.0	272.3	8.85
0.711	1238	73.7	132.5	267.4	9.25
1.10	1253	72.7	121.7	271.0	8.40
1.28	1193	73.3	116.8	260.8	8.30
2.155	1320	70.7	106.5	264.8	8.38
2.36	1308	71.3	104.3	265.8	8.10
3.965	1425	80.0	105.2	277.0	8.31
5.38	1468	81.3	101.9	273.3	8.6
5.44	1468	79.0	99.3	271.0	8.6
(Re = 27,400; W = 59.0 lb/hr)					
0.244	1983	75.0	135.1	267.7	15.0
0.521	2110	75.7	129.8	273.6	14.7
0.551	2130	76.3	130.2	274.3	14.8
0.580	2020	74.0	123.9	262.8	14.6
0.603	2055	76.0	126.2	268.0	14.6
0.695	2140	68.0	117.8	265.0	14.8
1.446	2030	79.0	113.0	264.5	13.4
1.467	2130	75.0	110.4	269.7	13.45
1.628	2035	78.0	110.1	263.8	13.25
2.97	2035	81.7	103.6	264.0	12.7

[a]Particle size = 200 μ

Table VIII

Local values of h(x/D/ h(46.4)[a]

W_s/W	h(46.4) BTU/hr ft^{2}F	Local h(x/D) / h(46.4) at x/D															
		0.704	1.41	2.82	4.23	5.64	7.04	8.44	12.6	16.9	21.1	25.4	29.6	33.8	38.0	42.3	46.4
(Re = 13,500; W = 29.0 lb/hr)																	
0.524	9.29	2.43	1.78	1.44	1.29	1.24	1.20	1.16	1.11	1.08	1.05	1.03	1.02	1.01	1.00	1.00	1.00
0.666	8.85	2.47	1.79	1.47	1.34	1.27	1.22	1.14	1.14	1.10	1.07	1.05	1.04	1.03	1.01	1.01	1.00
0.711	9.25	2.46	1.81	1.46	1.33	1.26	1.21	1.19	1.13	1.09	1.06	1.04	1.03	1.01	1.01	1.00	1.00
1.10	8.40	2.60	1.89	1.53	1.37	1.31	1.26	1.22	1.15	1.11	1.08	1.06	1.04	1.03	1.02	1.01	1.00
1.28	8.30	2.56	1.89	1.54	1.40	1.32	1.28	1.22	1.17	1.12	1.09	1.06	1.05	1.03	1.02	1.01	1.00
2.155	8.38	2.60	1.92	1.56	1.40	1.33	1.28	1.24	1.17	1.12	1.08	1.06	1.04	1.03	1.02	1.01	1.00
2.36	8.10	2.62	1.95	1.57	1.43	1.35	1.29	1.25	1.18	1.13	1.09	1.07	1.05	1.03	1.02	1.01	1.00
3.965	8.31	2.74	1.96	1.55	1.42	1.32	1.27	1.23	1.14	1.10	1.06	1.04	1.03	1.02	1.01	1.01	1.00
5.38	8.60	2.94	2.04	1.58	1.42	1.33	1.26	1.22	1.14	1.09	1.06	1.04	1.02	1.01	1.01	1.01	1.00
5.44	8.60	2.35	1.94	1.53	1.39	1.30	1.25	1.21	1.12	1.08	1.05	1.03	1.02	1.01	1.01	1.00	1.00
(Re = 27,400; W = 59 lb/hr)																	
0.244	15.0	2.11	1.63	1.39	1.29	1.24	1.21	1.18	1.11	1.07	1.06	1.05	1.03	1.02	1.01	1.01	1.00
0.521	14.7	2.20	1.68	1.42	1.32	1.27	1.22	1.20	1.14	1.11	1.08	1.06	1.04	1.03	1.01	1.01	1.00
0.551	14.8	2.19	1.68	1.42	1.32	1.27	1.22	1.20	1.14	1.10	1.07	1.06	1.04	1.03	1.02	1.01	1.00
0.580	14.6	2.20	1.71	1.44	1.34	1.28	1.23	1.21	1.14	1.11	1.08	1.06	1.04	1.03	1.01	1.01	1.00
0.603	14.6	2.22	1.71	1.45	1.35	1.28	1.24	1.21	1.14	1.11	1.08	1.06	1.04	1.03	1.01	1.01	1.00
0.695	14.8	2.16	1.68	1.42	1.32	1.26	1.22	1.19	1.13	1.09	1.06	1.04	1.03	1.01	1.01	1.00	1.00
1.446	13.4	2.40	1.83	1.54	1.42	1.35	1.31	1.27	1.19	1.14	1.10	1.08	1.06	1.04	1.02	1.01	1.00
1.467	13.5	2.42	1.85	1.55	1.44	1.38	1.32	1.27	1.20	1.15	1.11	1.08	1.06	1.03	1.02	1.01	1.00
1.628	13.3	2.40	1.85	1.56	1.43	1.36	1.31	1.27	1.20	1.15	1.11	1.08	1.06	1.04	1.03	1.01	1.00
2.970	12.7	2.51	1.90	1.58	1.45	1.38	1.32	1.29	1.20	1.15	1.10	1.08	1.06	1.04	1.03	1.01	1.00

[a]Bead size = 200 μ

Table IX

Two-phase friction factors [a]

W_s/W	$G_m \times 10^{-4}$ lb/hr ft^2	Inlet pressure $\times 10^{-3}$ psta	Pressure drop psf	T_{av} ^oR	f
(Re = 13,500					
0.247	1.31	2.07	4.1	572.8	.00704
0.265	1.33	2.07	4.1	571.4	.00694
0.266	1.33	2.07	4.1	569.8	.00506
0.272	1.34	2.07	4.1	569.0	.00500
0.429	1.53	2.06	7.0	565.1	.01070
0.57	1.65	2.06	4.1	567.5	.00540
0.58	1.66	2.06	4.1	563.8	.00550
0.78	1.80	2.06	7.0	561.0	.00980
0.95	2.04	2.05	4.1	554.7	.00472
1.15	2.26	2.05	4.1	555.2	.00414
1.17	2.28	2.05	4.1	554.3	.00412
3.20	4.44	2.01	9.1	550.6	.00486
5.96	7.35	1.95	16.5	564.7	.00505
6.85	8.30	1.94	18.9	560.6	.00530
(Re = 27,400)					
0.45	3.05	1.97	13.2	566.4	.00455
0.51	3.18	1.96	13.6	566.0	.00438
0.74	3.65	1.94	14.0	558.3	.00408
1.14	4.51	1.90	14.0	558.7	.00307
1.50	5.25	1.83	15.2	559.6	.00272
3.50	9.45	1.70	24.7	551.0	.00231

[a] Particle size = 30 μ

Table X

Two-phase friction factors[a]

W_s/W	$G_m \times 10^{-4}$ lb/hr ft^2	Inlet pressure $\times 10^{-3}$ psta	Pressure drop psf	T_{av} °R	f
(Re = 13,500)					
0.524	1.60	2.07	4.1	567.6	.00570
0.666	1.76	2.06	4.1	563.3	.00518
0.711	1.80	2.06	4.1	565.4	.00508
1.10	2.21	2.06	4.9	559.1	.00508
1.28	2.40	2.07	5.3	556.7	.00518
2.155	3.32	2.06	6.2	549.9	.00445
2.36	3.53	2.05	6.2	549.2	.00422
3.965	5.22	2.02	8.2	553.4	.00333
5.38	6.70	2.01	8.6	552.2	.00302
5.44	6.77	2.01	8.6	549.8	.00300
(Re = 27,400)					
0.244	2.66	1.98	13.2	567.5	.00512
0.521	3.25	1.93	14.8	564.9	.00455
0.551	3.32	1.93	14.8	565.4	.00444
0.580	3.38	1.96	14.4	560.9	.00441
0.603	3.43	1.96	14.4	563.1	.00432
0.695	3.62	1.96	14.7	554.9	.00420
1.446	5.24	1.89	18.1	557.3	.00347
1.467	5.28	1.93	17.3	564.0	.00327
1.628	5.63	2.03	17.7	555.2	.00346
2.97	8.48	1.96	22.2	553.4	.00278

[a]Particle size = 200 μ

APPENDICES

A. Details of Experimental Equipment

The following equipment was used in the two-phase heat transfer experiment:

Heated Section.

The heated section was 3/4-in. (0.710 in. i.d.) type 304 stainless steel tube, 35.55 inches long. Thermocouples were installed on opposite sides of the tube as shown in Fig. 2. Terminal flanges were 3-in. diam $\times$ 1/8-in. thick copper plates which were silver soldered to the tube ends. Four 1/4-in. brass studs were threaded through the copper discs and silver soldered in place for electrical connections.

Test Section End Connections.

The end fittings were machined from Bakelite as shown in Fig. 2. The heated tube protruded into the Bakelite to obtain proper alignment. Two opposing 1/32-in. holes were drilled through the inside wall for pressure taps. Both fittings were bored to the outside diameter of the stainless steel tube to a depth of 1-in. to receive the approach section and adiabatic tubes. This procedure assured accurate alignment of the flow at inlet and outlet. The Bakelite was accurately machined to provide the best possible continuity of flow.

Approach Section.

The approach section was taken from the same piece as the heat transfer section. It is 24-in. long and is preceded by a 3/8-in. diam Venturi nozzle. The nozzle was necessary to redistribute the solid phase which was concentrated at the outside tube wall following the 90^{o} turn. An iron-constantan thermocouple was spot-welded to the outside tube wall 2-1/2-in. before the heated test section inlet. This thermocouple measured the mixture inlet temperature. The approach section was insulated with 1 in. of 85% magnesia to prevent heat loss or gain to the room.

Adiabatic Section.

About 48 in. of stainless steel tubing (taken from the same piece as the heated section) followed the test section. Thermocouples were spot-welded to one side at the locations shown in Fig. 2. This section was insulated as described below.

Insulation.

The heated and adiabatic sections were insulated with 4 in. and 3 in. respectively of Santo-Cel powdered insulation. The insulation was contained by two cylinders made of galvanized sheet. The lower can was supported at the bottom by a Bakelite flange which was connected to Bakelite terminal flange as shown in Fig. 2. A 3.50-8 inflated rubber inner tube, located between the two cylinders (at the point where current leads and pressure tubing were led out), effectively contained the powdered insulation. The top of the upper cylinder was covered with sheet Bakelite sealed to the stainless steel tube with an "O" ring gasket.

Transformer.

Current to the heated tube was provided by a transformer.* Rated as follows: 60 cycles /sec 1-phase. Primary: 110/220 volts, 22/11 amps. Secondary: 8 volts, 300 amps. The primary side was controlled by a Variac variable auto-transformer.

Voltmeter.

The voltmeter was made by Weston Electrical Instrument Company and was calibrated before use. It is rated at 25-125 cycles for 5/10 volts. Its resistance for 5 volts is 20.3 ohms, and for 10 volts 40.7 ohms. The full scale deflection is 5 in.

Ammeter.

The ammeter, calibrated before use, was made by Western Electro-Mechanical Co., Oakland. It is used for currents from 2 to 200 amps and has a full scale deflection of 6 in.

Thermocouples.

Iron-constantan 30-gauge duplex wire was butt-welded to form thermocouples. On one side of the heated tube they were spot-welded

---

*Made by Engineering Works of Oakland, California.

to the tube metal and wrapped with two turns of glass cloth adhesive tape. On the other side they were insulated with 0.001 in. of Mylar plastic and then wrapped with tape. In both cases, the lead wires extended circumferentially one-quarter of the distance around the tube to minimize conduction in the lead wires.

Potentiometer.

Thermo-electric potential readings from the thermocouple system were recorded by a single point Brown Electronic recorder having a range 0-5 mv. For potentials larger than 5 mv, the system was bucked with a Leeds and Northrup student-type potentiometer, 0.1 mv least count. This bucking potentiometer was set at 5 mv with a Leeds and Northrup model 8662 potentiometer, 0.01 mv least count. The bucking voltage and recorder were regularly checked with the model 8662 to guarantee readings to the accuracy of the recorder (0.02 mv, 2/3 F for iron-constantan; readings were interpolated to 0.01 mv).

Weigh Tank and Scales.

The solids capacity of the aluminum scale tank was 200 lb. The scale had a capacity of 200 lb and produced a noticeable deflection for 0.05 lb. change in weight.

Air Metering Nozzle.

Air was metered with a standard ISA nozzle. Calculations of air rate versus pressure drop are presented in detail in Reference 2. Pressure difference measurements were made with an inclined Ellison-draft gage.

B. Experimental Accuracy

The maximum error in a function $F(x, y, z, \ldots)$ is given by

$$\frac{dF}{F} = \frac{1}{F}\left(\frac{\partial F}{\partial x}\,dx + \frac{\partial F}{\partial y}\,dy + \frac{\partial F}{\partial z}\,dZ + \ldots\right)$$

The heat transfer coefficient was calculated from the following formula

$$h = \frac{q}{T_0 - T_{mm}}$$

where $$T_{mm} = T_1 + \frac{\pi D q x}{W_c + W_s c_s}$$

The following table of information was used in the error calculation:

Variable	Base Value		Estimated Deviation
	low flow	high flow	
L, in.	35.55	35.55	0.05
D, in.	0.710	0.710	0.003
voltage, v	2.25	3.30	0.02
current, amps	90	134	2
T_1 °F	70	70	0.33
T_0 °F	128	276	0.33
x, in.	12	12	0.05
W, lb/hr	29	59	1.5
total wt, of solids, lb	2	23	0.05
feeding time, sec	474	408	0.2

The maximum error in the value of the heat transfer coefficient was found to be 4.4% at the low flow rate and 3.1% at the high flow rate.

C. Flowing Gas-Solids Mixtures Experiments in an Isothermal Tube

Solid spherical particles, 30 μ in diameter were added to an air stream flowing in 17 mm i.d. glass tubing. This phase was an extension of the experiments performed for the author's M.S. thesis, Reference 3. The solids feeding and recovery system, and air pumping and metering system, are the same as was used in the constant heat flux apparatus which has been described in Section II.

Condensing carbon tetrachloride vapors maintained the vertically mounted heat transfer tube at a constant temperature. The heat transfer system consisted of a 5-liter pyrex vapor generating flask heated by a gas burner, a thermally insulated and electrically heated vapor line to the jacketed pyrex heat exchanger, and a condensate return to the vapor generator through the 250-cc jacketed buret. The pressure control condenser received vapor from the top of the heat exchanger opposite to the vapor inlet through a pneumatically operated pressure control valve. The pressure control valve was actuated by a Fisher Wizard controller. Condensate returned continuously from the condenser to the vapor generator through a globe check valve by the pressure in the condenser and its own hydrostatic head. The closed chromate-treated cooling water system maintained the desired pressure in the condenser. The experimental heat exchanger was made of selected thick-walled pyrex tubing fitted to monel-metal headers by Teflon gaskets. The insulating and heat transfer chambers were open to each other at the top to maintain the same pressure in both. The exchanger has the following significant dimensions:

heat transfer tube	- 20 mm o.d. × 17 mm i.d.
	- 31-3/4 in. length
	- 0.4636 sq. ft. area based on i.d.
outer jacket	- 3 in. o.d.
inner jacket	- 1-27/32 in. o.d.

Condensate and vapor in the insulating jacket flowed to the buret jacket, thereby minimizing heat loss from the buret. The condensate resulting from heat transfer to the solids-gas mixture was collected in the buret and returned to the vaporizor after each run. The 1-3/8 in. o.d. pyrex buret and 2-3/8 in. o.d. pyrex jacket were fitted to Everdur metal headers by Teflon gaskets. The vent gas holder, telescopic type with a heavy oil seal, held the nitrogen used to blanket the vapor volume when the system was not in operation.

The heat rate to the mixture was calculated by multiplying the condensate rate by the latent heat of vaporization. The resistance of the condensate film and tube wall was measured during the air calibration tests.

Bulk mean inlet and exit air temperatures were measured with thermocouples directly in the air stream.

The above data were converted to overall heat transfer coefficients based on the logarithmic mean temperature difference. The results of these calculations are shown in Fig. 21 for the two constant air Reynolds numbers. The scatter in the points is about 20%, but the relationship of heat transfer coefficient to solids loading ratio is clearly defined.

D. Theoretical Analysis

Theory derived from the energy equation

The purpose of the work in this appendix is to find an analytical expression for predicting the heat transfer characteristics of the gas-solids flow system. The system to be analyzed is restricted by the following assumptions.

1. The two-phase flow system is fully developed at the pipe inlet.
2. Solid particles and gas are at the same temperature at the pipe inlet.
3. The solid phase is uniformly distributed throughout the pipe cross section.
4. The solid particle concentration is so lean that there is no effect on the mean and fluctuating velocity of the continuous phase.
5. The particles are spheres of uniform size and travel at the local gas velocity.
6. Radiation effects are neglected.
7. Fluid properties are constant and uniform.
8. The particle Biot number is small enough to neglect radial variation of temperature within the sphere.
9. The heat flux at the pipe wall is uniform.
10. Axial diffusion of heat is negligible compared to radial diffusion.
11. Viscous dissipation is negligible.

Derivation of Equations

The derivation of the heat balance and energy equations is due to Tien.[20] Considering a unit volume element containing n_s solid particles, the energy balance in polar coordinates can be written as

$$\rho c u \frac{\partial T}{\partial x} = \frac{1}{r} \frac{\partial}{\partial r} \left[r(k+\rho c \epsilon_H) \frac{\partial T}{\partial r} \right] + n_p h_p A_p (T_s - T) \qquad (1)$$

where the mean radial and aximuthal velocities are assumed to be zero. Using the analogy between heat and momentum transport, $\epsilon_H = \epsilon_m$, Eq. (1) can be further written as

$$u \frac{\partial T}{\partial x} = \frac{1}{r} \frac{\partial}{\partial r} \left[r \nu \gamma \frac{\partial T}{\partial r} \right] - K_1 (T - T_s) \qquad (2)$$

where

$$\gamma = \nu (a + \epsilon_m)$$

$$K_1 = n_p \frac{Nu_p a}{\partial a} A_p$$

The validity of the assumption $\epsilon_H = \epsilon_m$ is thought to be reasonable in the light of the current uncertainty as to their precise nature. Also, their equivalence can be shown in terms of the statistical properties of turbulence.[19]

The heat balance equation between the solid particles and gas phase is

$$\rho_p c_s V_p u \frac{\partial T_s}{\partial x} = h_p A_p (T - T_s) \qquad (3)$$

This heat balance can be written as

$$u \frac{\partial T_s}{\partial x} = K_2 (T - T_s) \qquad (4)$$

where

$$K_2 = \frac{Nu_p k A_p}{z \rho_p c_s V_s a}$$

The boundary conditions for $T(x, r)$ and $T_s(x, r)$ are as follows:

$$\left.\begin{aligned} T(0, r) &= T_1 \quad ; \quad -k \frac{\partial T}{\partial r}(x, r_0) = q \\ T_s(0, r) &= T_1 \quad ; \quad \frac{\partial T}{\partial r}(x, 0) = 0 \end{aligned}\right\} \tag{5}$$

With the dimensionless variable

$$\theta = \frac{T - T_1}{\frac{q\, r_0}{k}} \qquad x^+ = \frac{x}{r_0}$$

$$u^+ = u/\sqrt{\tau_0/\rho} \qquad r^+ = r\sqrt{\tau_0/\rho}/\nu$$

Equations (2), (4), and (5) become

$$u^+ \frac{\partial \theta}{\partial x^+} = \frac{r_0^+}{r^+} + \frac{\partial}{\partial r^+}\left\{ r^+ \gamma \frac{\partial \theta}{\partial r^+} \right\} + K_1 \frac{\nu r_0^+}{\tau_0/\rho} (\theta_s - \theta) \tag{6}$$

$$u^+ \frac{\partial \theta_s}{\partial x^+} = r_0^+ K_2 \frac{\nu}{\tau_0/\rho} (\theta - \theta_s) \tag{7}$$

$$\left.\begin{aligned} \theta(0, r^+) &= 0 \qquad \frac{\partial \theta}{\partial r^+}(x^+, r_0^+) = \frac{1}{r_0^+} \\ \theta_s(0, r^+) &= 0 \qquad \frac{\partial \theta}{\partial r^+}(x^+, 0) = 0 \end{aligned}\right\} \tag{8}$$

Entry and fully developed solutions

Following the technique employed by Sparrow[18] for a homogenous fluid, the temperature solutions for both phases will be separated into two parts.

$$\theta = \theta_1 + \theta_2$$

θ_1 is the fully developed solution that is attained far down the pipe where similar temperature profiles persist. θ_2 is the remainder after θ_1 has

been subtracted. For a single phase fluid it is obvious that

$$\lim_{x^+ \to \infty} \theta_2 = 0$$

The same procedure is applied to θ_s, i.e.,

$$\theta_s = \theta_{1s} + \theta_{2s}$$

Fully developed solution

Since (6) and (7) are linear, θ_1 and θ_{1s} can be applied separately.

$$u^+ \frac{\partial \theta_1}{\partial x^+} = \frac{r_0^+}{r^+} \frac{\partial}{\partial r^+} \left\{ r^+ \gamma \frac{\partial \theta_1}{\partial r^+} \right\} + K_1 \frac{\nu r_0^+}{\tau_0/\rho} (\theta_{1s} - \theta_1) \qquad (9)$$

$$u^+ \frac{\partial \theta_{1s}}{\partial x^+} = K_2 \frac{\nu r_0^+}{\tau_0/\rho} (\theta_1 - \theta_{1s}) \qquad (9a)$$

Boundary conditions (8) become $\frac{\partial \theta_1}{\partial r^+}(r_0^+, x^+) = \frac{1}{r_0^+}$; $\frac{\partial \theta_1}{\partial r^+}(0, x^+) = 0$ (10)

As a consequence of the definition of θ_1,

$$\frac{\partial \theta_1}{\partial x^+} = \text{constant.} \qquad (11)$$

To calculate the value of this constant, we define a mixed mean temperature, T_{mm}. The total energy in the stream is

$$\int_0^{r_0} 2\pi r u \rho c T dr + \int_0^{r_0} 2\pi r u \rho_s c_s T_s dr \equiv (Wc + W_s c_s) T_{mm}$$

or

$$T_{mm} = \frac{Wc}{Wc + W_s c_s} T_m + \frac{W_s c_s}{Wc + W_s c_s} T_{ms}$$

T_{mm} is also given by an energy balance which can be put in the dimensionless form

$$\theta_{mm} = \frac{T_{mm}-T_1}{\frac{qr_0}{k}} = \frac{2\pi x k}{Wc+W_s c_s} ;$$

therefore

$$\theta_{mm} = \frac{4}{Pe_m} x^+ \qquad (15)$$

where $$Pe_m = RePr\left(1 + \frac{W_s c_s}{W c}\right)$$

Now far down the pipe

$$\frac{\partial T_{mm}}{\partial x} = \frac{\partial T_m}{\partial x} = \frac{\partial T_s}{\partial x}$$

so that $$\frac{\partial \theta_1}{\partial x^+} = \frac{4}{Pe_m}$$

and $$\theta_1 = \frac{4}{Pe_m} x^+ + H_1(r_0^+) + A \qquad (16)$$

We would like to have $H_1(r_0^+)$ correspond to Sparrow's function $G(r_0^+)$. A condition on G for single phase flow is

$$\int_0^{r_0} Gurdr = 0$$

We will determine A so that

$$\int_0^{r_0} H_1 rudr = 0.$$

Using Eq. (16), it is found that

$$A = (\theta_m - \theta_{mm})_\infty$$

the difference between the mixed mean of the gas and the total mixed mean evaluated far down the pipe.

The complete expression for θ_1 becomes

$$\theta_1 = \frac{4}{Pe_m} x^+ + H_1(r_0^+) + (\theta_m - \theta_{mm})_\infty \tag{16a}$$

By similar reasoning, it is found that

$$\theta_{1s} = \frac{4}{Pe_m} x^+ + H_2(r^+) + (\theta_{ms} - \theta_{mm})_\infty \tag{17}$$

θ_1 and θ_{1s} can now be substituted into the energy balance Eq. (9) and heat balance Eq. (9a).

$$u^+ \frac{4}{Pe_m} = \frac{r_0^+}{r^+} \frac{d}{dr^+}\left\{r^+ \gamma \frac{dH_1}{dr^+}\right\} + K_1 \frac{\nu r_0^+}{\tau_0/\rho}\left\{(H_2 - H_1) - (\theta_{ms} - \theta_m)_\infty\right\} \tag{18}$$

$$u^+ \frac{4}{Pe_m} = K_2 \frac{\nu r_0^+}{\tau_0/\rho}\left\{(H_2 - H_1) - (\theta_{ms} - \theta_m)_\infty\right\} \tag{19}$$

Combining (18) and (19)

$$u^+ \frac{4}{Pe_m}\left(1 + \frac{W_s c_s}{W c}\right) = \frac{r_0^+}{r^+} \frac{d}{dr^+}\left\{r^+ \gamma \frac{dH_1}{dr^+}\right\} \tag{20}$$

where

$$\frac{K_1}{K_2} = n_s V_s \frac{p_s c_s}{p c} = \frac{W_s c_s}{W c} \tag{21}$$

But since

$$Pe_m = Pe\left(1 + \frac{W_s c_s}{W c}\right)$$

(20) can be written simply as

$$u^+ \frac{4}{Pe} = \frac{r_0^+}{r^+} \frac{d}{dr^+}\left\{r^+ \gamma \frac{dH_1}{dr^+}\right\} \tag{22}$$

and the boundary conditions (10) become

$$\frac{dH_1}{dr^+}(r_0^+, x^+) = \frac{1}{r_0^+} \; ; \; \frac{dH_1}{dr^+}(0, x^+) = 0 \qquad (23)$$

Equation (19) gives the relationship between H_1 and H_2. With the help of the boundary conditions Eq. (23), the condition for θ_{1s} can be stated.

$$\frac{\partial \theta_{1s}}{\partial r^+}(x^+, r_0^+) = \frac{dH_2}{dr^+}(x^+, r_0^+) = \frac{1}{r_0^+} - \frac{4}{Pe_m} \frac{\tau_0/\rho}{K_2 \nu r_0^+}$$

$$\frac{\partial \theta_{1s}}{\partial r^+}(x^+, 0) = 0$$

Equation (22) with (23) is identical to Sparrow's Eq.(5a). The solution to (22) was carried out by him using the turbulent velocity profile of Deissler [2]. The expression used for γ is given in [18], and numerical calculations were performed for Reynolds numbers of 50,000; 100,000; and 500,000 for Prandtl numbers of 0.7, 10, and 100.

Entry region solution

As previously reasoned for θ_1 and θ_{1s}, θ_2 and θ_{2s} also satisfy the energy and heat balance Eqs. (6) and (7)

$$u^+ \frac{\partial \theta_2}{\partial x^+} = \frac{r_0^+}{r^+} \frac{\partial}{\partial r^+} \left\{ r^+ \gamma \frac{\partial \theta_2}{\partial r^+} \right\} + K_1 \frac{\nu r_0^+}{\tau_0/\rho} (\theta_{2s} - \theta_2) \qquad (24)$$

$$u^+ \frac{\partial \theta_{2s}}{\partial x^+} = K_2 \frac{\nu r_0^+}{\tau_0/\rho} (\theta_2 - \theta_{2s}) \qquad (25)$$

since

$$\frac{\partial \theta}{\partial r^+} = \frac{\partial \theta_1}{\partial r^+} + \frac{\partial \theta_2}{\partial r^+} \; ,$$

$$\frac{\partial \theta_2}{\partial r^+}(x^+, r_0^+) = 0; \; \frac{\partial \theta_2}{\partial r^+}(x^+, 0) = 0 \qquad (26)$$

and since

$$\theta(0, r^+) = 0 \quad \text{and} \quad \theta_1(0, r^+) = H_1(r^+),$$

$$\theta_2(0, r^+) = - H_1(r^+) \tag{26a}$$

The technique of separation of variables–as proposed by Tien[20]–will be used for the solution of (24)

$$\theta_2 = \mathfrak{C}\, \chi(x^+)\, \psi(r^+)$$

$$\theta_{2s} = \mathfrak{C}_s\, \chi(x^+)\, \psi_s(r^+) \tag{27}$$

Substituting (27) into (24) results in

$$\frac{\chi'}{\chi} = \frac{\frac{r_0^+}{r^+}\frac{d}{dr^+}\left(r^+ \gamma \frac{d\psi}{dr^+}\right)}{u^+(r^+)\,\psi(r^+)} + \frac{\Gamma}{u^+(r^+)}\left(\frac{\mathfrak{C}_s \psi_s}{\mathfrak{C}\psi} - 1\right) = - \frac{2B_n^{\,2}}{Re} \tag{28}$$

where

$$\Gamma = K_1 \frac{\nu r_0^+}{\frac{\tau_0}{\rho}}$$

Equation (28) can be integrated immediately.

$$\chi = \exp\left[- \frac{2B_n^{\,2}}{Re}\, x^+ \right] \tag{29}$$

If (27) is applied to the heat balance Eq. (25), the result is

$$\frac{\chi'}{\chi} = - \frac{\Omega}{u^+(r^+)}\left(1 - \frac{\mathfrak{C}\psi}{\mathfrak{C}_s \psi_s}\right) = - \frac{2B_n^{\,2}}{Re} \tag{30}$$

where

$$\Omega = \frac{K_2\, \nu r_0^+}{\tau_0/\rho}$$

Rewriting (28) and substituting $\mathfrak{C}\psi/\mathfrak{C}_s\psi_s$ from (30) yields

$$\frac{\dfrac{d}{dr^+}\left(r^+\gamma\dfrac{d\rho}{dr^+}\right)}{\dfrac{r^+ u^+ \psi}{r_0^+}} + \frac{\Gamma}{u^+}\left(\frac{1}{1 - \dfrac{2B_n^{\,2} u^+}{\Omega\, Re}} - 1\right) = -\frac{2B_n^{\,2}}{Re} \qquad (31)$$

The relationship between $C\psi$ and $C_s\,\psi_s$ can be written from Eq. (30).

$$C\psi = C_s\,\psi_s\left(1 - \frac{2B_n^{\,2}\,u^+}{Re\,\Omega}\right)$$

The boundary conditions on θ_{1s} may be found with the help of this equation and the boundary conditions on θ_1 :

$$\frac{\partial\theta_{2s}}{\partial r^+}(x^+, r_0^+) + \theta_{2s}(x^+, r_0^+)\,\frac{2B_n^{\,2}}{Re\Omega} = 0$$

$$\frac{\partial\theta_{2s}}{\partial r^+}(x^+, 0) = 0$$

In its present form (31) does not yield a solution by any known mathematical technique. If, however,

$$\frac{2B_n^{\,2}\,u^+}{\Omega\,Re} \ll 1 \qquad (32)$$

so that

$$\frac{1}{1 - \dfrac{2B_n^{\,2}u^+}{\Omega\,Re}} \approx 1 + \frac{2B_n^{\,2}\,u^+}{\Omega\,Re}$$

(31) takes the form

$$\frac{d}{dr^+}\left(r^+\gamma\ \frac{d\psi}{dr^+}\right)+\left(\frac{W_s c_s}{Wc}+1\right)\left(\frac{2B_n^{\,2}}{Re}\ \frac{r^+}{r_0^+}\right)\psi=0 \tag{33}$$

where $$\frac{\Gamma}{\Omega}=\frac{W_s c_s}{Wc}$$

The validity of (32) will be analyzed later because a knowledge of the eigenvalues $B_n^{\,2}$ is required.

Defining $\beta_n^{\,2}$ by

$$\beta_n^{\,2}=\left(1+\frac{W_s c_s}{Wc}\right)B_n^{\,2} \tag{34}$$

reduces Eq. (33) to

$$\frac{d}{dr^+}\left(r^+\gamma\ \frac{d\psi}{dr^+}\right)+\left(\frac{2\beta_n^{\,2}}{Re}\ \frac{r^+}{r_0^+}\ u^+\right)\psi=0 \tag{35}$$

Equation (35) with its boundary conditions

$$\left.\begin{aligned}\frac{\partial\theta_2}{\partial r^+}(x^+,\ 0)&=\frac{d\psi}{dr^+}(0)=0\\ \frac{\partial\theta_2}{\partial r^+}(x^+,\ r_0^+)&=\frac{d\psi}{dr^+}(r_0^+)=0\end{aligned}\right\} \tag{36}$$

is an eigenvalue problem of the Sturm-Liouville type. Solutions are possible for a discrete set of eigenvalues. Sparrow has found the first six eigenvalues and eigenfunctions by numerical integration, and these are reported in Reference 18.

The coefficients C_n are determined to satisfy the initial condition (26a). From the orthogonality property of the Sturm-Liouville system it

follows that

$$C_n = \frac{\int_0^{r_0^+} \left[-H_1(r^+)\right] r^+ u^+ \psi_n \, dr^+}{\int_0^{r_0^+} r^+ u^+ \psi_n^2 \, dr^+} \tag{37}$$

The complete temperature solution for the gas phase can now be written as

$$\theta = \frac{4}{Pe_m} x^+ + H_1(r^+) + (\theta_m - \theta_{mm})_\infty + \sum C_n \psi_n(r^+) \exp\left[\frac{2\beta_n^2 x/D}{Re(1+\frac{W_s c_s}{W c})}\right] \tag{38}$$

Notice that the expression is identical to the single phase flow result with the exception of the heat capacity loading term in the exponential and the term $(\theta_m - \theta_{mm})_\infty$.

Return now to examine the assumption previously made that

$$\frac{2 B_n^2 u^+}{\Omega Re} \ll 1 \tag{32}$$

where

$$\frac{2u^+}{\Omega Re} = \frac{2}{3} \frac{\nu}{k} \frac{a^2}{r_0^2} \frac{\rho_p c_s}{Nu_p} \frac{u}{u_m} \tag{39}$$

For the experimental system concerned in this work

$$\frac{2}{3} \frac{\nu}{r^2} \frac{\rho_p c_s}{k} = 9.6 \times 10^5 \text{ ft}^{-2}$$

Values of Nu_p can be estimated the relative velocity measurements of Meyer[9] and the correlation

$$Nu_p = 2 + 0.492 \sqrt{Re_p} \qquad 10 < Re_p < 1.8 \times 10^3$$

proposed by Yuge.[23]

The following table was constructed in terms of β_n^2 while restricting $\frac{W_s}{W}$ to values less than one.

$$\beta_n^2 \ll \begin{cases} 1500\frac{u_m}{u} & \text{particle size } 30 & \text{Re all} \\ 100\frac{u_m}{u} & \text{particle size } 200 & \text{Re } 13{,}500 \\ 140\frac{u_m}{u} & \text{particle size } 200 & \text{Re } 27{,}400 \end{cases}$$

Sparrow's eigenvalues were extrapolated to lower Reynolds numbers for $Pr = 0.7$

	β_0^2	β_1^2	β_2^2	β_3^2	β_4^2	β_5^2
Re = 13,500	0	440	1150	2200	3600	5200
Re = 27,400	0	620	2200	4100	6650	9800

It can be readily seen that the inequality (32) is true only for the first eigenvalue and is approximately valid near the pipe wall for the smaller size particles.

Further significance can be attached to this assumption by returning to Eq. (30), which can be rewritten as

$$\frac{C\psi}{C_s\psi_s} = 1 - \frac{2B_n^2 u^+}{Re\,\Omega}$$

But, using the inequality (32),

$$\frac{C\psi}{C_s\psi_s} \approx 1$$

The real sacrifice made for reducing Eq. (31) to the Sturm-Liouville system was to say that both phases are at about the same temperature!

Heat transfer results

Define a heat transfer coefficient

$$h = \frac{q}{T_0 - T_{mm}} \tag{39a}$$

and Nusselt number

$$Nu_s = \frac{2hr_0}{k} = \frac{2}{\theta_0 - \theta_{mm}} \tag{40}$$

where

$$\theta_{mm} = \frac{4x^+}{Pe_m} \tag{40a}$$

Using (38), the Nusselt number can be evaluated as

$$Nu_s = \frac{2}{H_1(r_0^+) + (\theta - \theta_{mm})_\infty + \Sigma C_n \psi_n(r_0^+) \exp\left[\frac{2\beta_n^2 x^+}{\left(1 + \frac{W_s c_s}{W c}\right) Re}\right]} \tag{41}$$

Far down the pipe the asymptotic Nusselt number becomes (since $C_o = 0$)

$$(Nu_s)_\infty = \frac{2}{H_1(r_0^+) + (\theta_m + \theta_{mm})_\infty} \tag{42}$$

With regards to the term $(\theta_m - \theta_{mm})_\infty$,
we write

$$T_m = T_{mm} = \frac{W_s c_s}{W_s c_s + W c} (T_m - T_{ms}) \tag{43}$$

for the flow far down the pipe.

The quantity $(T_m - T_{ms})$ is not easily expressed in terms of the particle heat transfer coefficient, and involves the integration of functions containing H_1 and H_2 which are not readily obtainable. If we assume that T and T_s have about the same profile,

$$T_m - T_{ms} \approx T - T_s = \frac{u_m}{K_2} \frac{\partial T_s}{\partial x}$$

Equation (4) has been used in the last step.

From a heat balance we find that

$$\frac{d\,T_{mm}}{dx} = \frac{2\pi\, r_0\, q}{Wc+W_s c_s},$$

and for the fully developed region

$$\frac{\partial T_s}{\partial x} = \frac{d\,T_{mm}}{dx}.$$

Combining these steps, the results

$$T_m - T_{mm} = \frac{W_s c_s}{W_s c_s+Wc} \left\{ \frac{u_m}{K_2} \quad \frac{2\pi\, q\, r_0}{W_s c_s+Wc} \right\}$$

The approximate form of the local Nusselt number is

$$\frac{2}{Nu_s} = H_1(r_0^+) + \frac{W_s c_s}{(W_s c_s+Wc)^2} \quad (2\pi\, r_0\, q\, u_m/K_2). \tag{44}$$

$$+ \Sigma\, C_n \psi_n(r_0^+) \exp \left[\frac{2\beta_n^2\, x^+}{\left(1+ \frac{W_s c_s}{Wc}\right) Re} \right]$$

The approximate form of the asymptotic Nusselt number is

$$\frac{1}{Nu_{s\infty}} = \frac{1}{Nu_\infty} + \frac{W_s c_s}{(W_s c_s+Wc^2)} \left\{ \pi\, k \quad \frac{u_m}{K_2} \right\} \tag{45}$$

Where Nu_∞ is the asymptotic Nusselt number for the single phase given by Sparrow.

The factor $\dfrac{W_s c_s}{(W_s c_s+Wc)^2}$ is zero at both high and low loading ratios. It has a maximum value at $(W_s c_s/Wc) = 1$ ($W_s/W = 1.26$ for glass particles and air).

For the two air rates used in the experiments are tabulated below

	maximum
Re = 13,500	0.0355
Re = 27,400	0.0175

Values of the factor $\pi k u_m/K_2$ for the experimental system are tabulated below.

particle size	Reynolds No.	
	13,500	27,400
30 μ	0.0116	0.0236
200 μ	0.52	1.05

K_2 is proportion to $1/a^2$, accounting for the large differences in the values for the two sizes.

For the 30μ particles, these numerical results combine to yield values of Nu_∞ that differ from $Nu_{s\infty}$ by less than 3% at both Reynolds Nos. For the 200 μ particles, the maximum decrease in the asymptotic Nusselt number

$$\frac{Nu_\infty - Nu_{s\infty}}{Nu_\infty} \quad (100) \qquad (46)$$

is 23%.

Neglecting the term $(\theta_m - \theta_{mm})_\infty$ for the 30 μ beads as is justified by the above numerical results, allows us to write the Nusselt number ratio in a simple form

$$\frac{Nu_s}{Nu_{s\infty}} = \frac{1}{1 + \Sigma A_n \exp\left[-\frac{2\beta_n^2 x^+}{Re\left(1+\frac{W_s c_s}{W c}\right)}\right]}$$

where $A_n = \dfrac{C_n \psi_n(r_0^+)}{H_1(r_0^+)}$ and has been evaluated by Sparrow.

Analogy between heat transfer and fluid friction

The previous section derives a solution based on the energy equation and the heat balance between the phases. The resulting expression states that the two-phase tube-wall Nusselt number is predicted on the basis of the wall shear stress for air alone. Since overall pressure drop measurements were made simultaneously with the heat transfer measurements, it is incumbent upon us to make some attempts to predict the heat transfer coefficient from the pressure drop.

According to Sparrow[18], Nu_∞ for air alone is a function only of r_0^+, where

$$r_0^+ = r_0 \frac{\sqrt{\tau_0/\rho}}{\nu} \tag{47}$$

The question is, how are Nu_∞ and r_0^+ functionally related ? Sparrow's results do not explicitly yield the relationship, but he does give Nu_∞ as a function of Reynolds number. It remains to find the relation between Re and r_0^+.

The definition of the friction factor, f, is

$$f \equiv \frac{\tau_0}{\rho_s u_m^2/2g} \tag{48}$$

where

$$\rho_s = \rho \left(1 + \frac{W_s}{W} \right)$$

The definition can be rearranged so that

$$f = \frac{8(r_0^+)^2}{Re_s^2} \tag{49}$$

where

$$Re_s = \frac{2\rho_s u_m r_0}{\mu}$$

It is assumed that the mixture acts as a homogeneous fluid, and we use the single phase relation

$$\frac{f}{2} = \frac{0.023}{Re_s^{0.2}} \tag{50}$$

Combining Eqs. (49) and (50) gives an equation that reduces to

$$r_0^+ = 0.0761 \; Re_s^{0.9} \tag{51}$$

This result is combined with Sparrows relation

$$Nu_\infty = 0.0245 \; Re^{0.77}, \; Pr = 0.7$$

to yield

$$Nu_\infty = 0.2255 \, (r_0^+)^{0.856} \tag{52}$$

If we let Nu_∞ be the Nusselt number for air alone, the ratio of the Nusselt number with solids to Nu_∞ is written:

$$\frac{(Nu_\infty)_s}{Nu_\infty} = \left(\frac{r_{0\,s}^+}{r_0^+} \right)^{0.856} \tag{53}$$

where r_0^+ is for air alone.

Going back to the definition of r_0^+, we see that we have the option of changing τ_0/ρ_s for the measured shear stress and leaving ν alone or of changing ν also, i.e., let

$$\nu_s = \nu / (1 + \frac{W_s}{W})$$

For the first case,

$$\frac{r_{0\,s}^+}{r_0^+} = \left[\frac{\Delta P_s}{\Delta P} \; / \; (1 + \frac{W_s}{W}) \right]^{1/2} \tag{54}$$

where Δp is measured for air alone and Δp_s is measured with solids present at the same air rate. Substituting Eq. (54) into (53) gives

$$\left(\frac{Nu_{\infty s}}{Nu_{\infty}}\right) = \left[\frac{\Delta P_s}{\Delta P} \cdot \frac{1}{\left(1 + \frac{W_s}{W}\right)}\right]^{0.428} \tag{55}$$

The above ratio is less than unity because the pressure drop does not increase as fast as the solids loading.

If we allow ν to change with solids loading as previously described,

$$\frac{(Nu_{\infty})_s^*}{Nu_{\infty}} = \left[\frac{\Delta P_s}{\Delta P} \cdot \left(1 + \frac{W_s}{W}\right)\right]^{0.428} \tag{56}$$

Values of $(Nu_{\infty})_s$ predicted by Eqs. (55) and (56) are compared to the experimental results in Figs. 21 and 22.

Equation (56) produces a greater Nusselt number because of the decrease in ν when the total density is used. The results obtained from Eq. (56) are so far from the experimental results that the idea is untenable.

E. A Method for Determining the Constant Heat Flux Thermal Entry Length in an Adiabatic Tube

The following development was suggested by Sparrow, Hallman and Siegel.[18] Their heat transfer results are extended to an adiabatic tube following a heated tube with the uniform heat flux boundary condition. It is assumed that this tube is of sufficient length to establish a fully developed temperature profile at its outlet.

The temperature is imagined to be composed to two solutions

$$\theta = \theta_1 + \theta_2$$

θ_1 is the solution far down the pipe where temperature profiles are similar. It satisfies the energy equation, has the following boundary condition

$$\frac{\partial \theta_1}{\partial r^+}(x^+, r_0^+) = \frac{1}{r_0^+}, \quad \frac{\partial \theta_1}{\partial r_0^+}(x^+, 0) = 0, \quad \frac{\partial \theta_1}{\partial x^+} = \text{constant}$$

and takes the following form in Sparrow's solution

$$\theta_1 = \frac{4}{Re\,Pr}\, x^+ + G(r^+)$$

θ_2 is the solution in the entry length and also satisfies the energy equation. It has the following boundary conditions

$$\frac{\partial \theta_1}{\partial r^+}(x^+, r_0^+) = 0, \quad \frac{\partial \theta_1}{\partial r^+}(x^+, 0) = 0,$$

and as a consequence of the inlet condition $\theta(0, r^+) = 0$,

$$\theta_2(0, r^+) = -G(r^+)$$

θ_2 takes the form

$$\theta_2 = \sum_{n=0}^{\infty} C_n \psi_n(r^+)\, e^{-\frac{2\beta_n^2 \chi^+}{Re}}$$

in Sparrow's solution.

The entrance condition on θ_2 gave rise to Sparrow's suggestion that it could be measured in an adiabatic section following a heated section. $G(r^+)$ is the fully developed temperature profile and could be measured under presumably better conditions where end effects are less severe.

The following figure illustrates these quantities as they exist in the combined system.

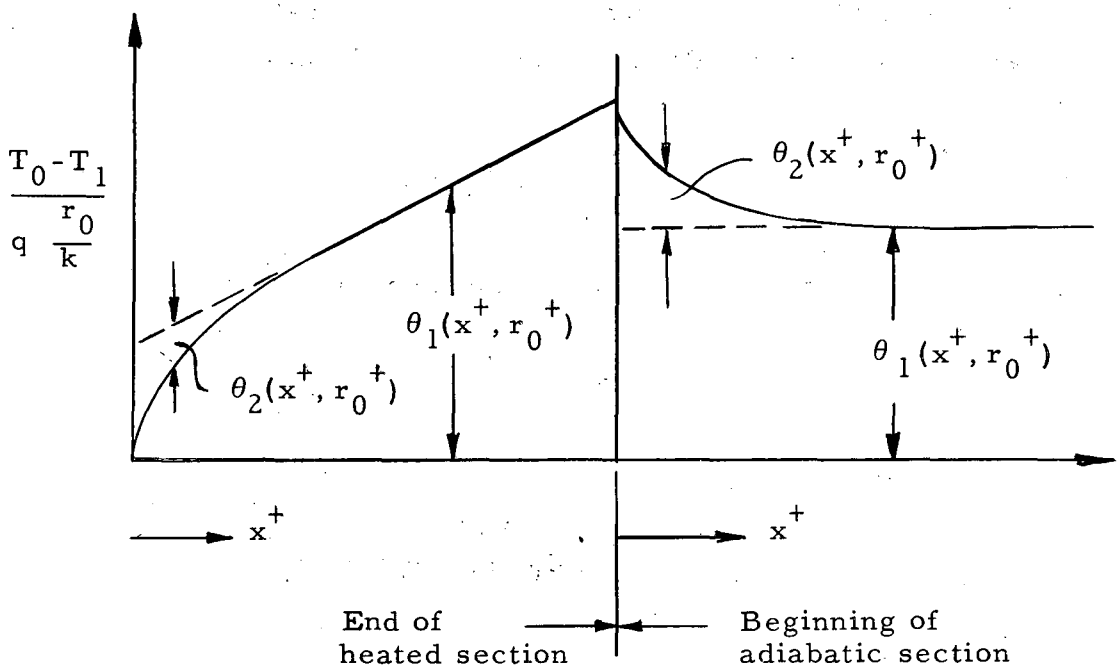

In terms of the quantities measured in this study,

$$\theta_2(x^+, r_0^+) = \frac{2}{Nu} \left(1 - \frac{h}{h_\infty} \right)$$ in the heated pipe and

$\theta_2(x^+, r_0^+) = \frac{2}{Nu}$ in the adiabatic section. The heat flux in the heated pipe is used in determining both Nusselt numbers.

F. Pressure Drop of a Two-Phase Mixture in a Heated Tube

Assuming that the solid phase is uniformly distributed and that the relative velocity between solids and gas is zero, the force balance is

$$dZ + v_m\, dP + \frac{4f}{D}\,\frac{u^2}{2g}\,dx + \frac{udu}{g} = 0.$$

Because of the above assumptions, the mixture mass velocity is

$$G_m = \frac{1}{v_m}\left(1 + \frac{W_s}{W}\right).$$

After some rearrangement, the force equation is

$$\frac{\left(1+\frac{W_s}{W}\right)}{RT} PdP + \frac{G_m{}^2 dv}{g\,v} = -\frac{1}{v_m{}^2}\left(\frac{4fu^2}{2Dg} + 1\right) dx$$

It is assumed that T is constant at the average of the two-phase mixture terminal temperatures. This assumption is justified because the variation of the absolute mixture temperature is less than 12% of the average and because T increases linearly with length.

It is also found that $4fu^2/2Dg \gg 1$ for our conditions. The severest test of this inequality appears at the lowest Reynolds number - 13,500-where $4fu^2/2Dg = 20$. After rearranging the force balance it can be integrated.

$$\frac{4fL}{D} = \frac{\left(\frac{W_s}{W}+1\right)}{G_m{}^2 RT_{ave}}\left(P_1{}^2 - P_2{}^2\right) - 2\ln\frac{P_1 T_2}{P_2 T_1}$$

For $W_s = 0$, the equation simplifies to the case for single phase flow. If the pressure drop and the temperature rise are not too large, the equation reduces to the incompressible flow case as follows:

$$\frac{P_1{}^2 - P_2{}^2}{R\,T_{ave}} \approx 2\,\frac{(P_1 - P_2)}{v}$$

and

$$\ln \frac{P_p T_2}{P_2 T_1} \approx 0$$

so

$$\frac{4fL}{D} \approx \frac{2gv}{u^2} (P_1 - P_2)$$

G. Sample Data and Calculations

Constants of the system

Length of heat transfer tube = 2.96 ft

Inside diameter = 0.710 inches

Heat transfer area = 0.551 sq. ft

Cross section flow area = 2.76×10^{-3} sq. ft

Determination of correction to measured heat input

Heat is lost non-uniformly from the heated section due to conduction through the electric leads and less effective thermal insulation at the ends. Regardless of this non-uniformity, a uniform correction to the measured heat input was used. This heat loss was based on the measured axial temperature gradient of the tube wall in the region where the gradient was constant (greater than 18"). The correction is given by

$$3.41\ EI - LWc \frac{dT}{dx}$$

E and I are the measured voltage and current, L is the tube length, W is the weight rate of air, c is the specific heat of air, and $\frac{dT}{dx}$ is the measured axial gradient. The error, calculated in this way, is equivalent to the radial heat loss through the insulation in the fully developed region. The values ranged from 45 to 24 BTU/hr with an average of 32 BTU/hr. The value of 30 BTU/hr was used in all heat transfer calculations.

Calculation of the local Nusselt number

The procedure is the same with or without solids. The following calculation is for run number RS-136, using 200 μ particles at Re = 13,500.

1. air rate = 29 lb/hr
2. solids rate = 62.5 lb/hr
3. $W_s/W = 2.16$
4. Measured heat input = 757 BTU/hr
5. net heat input = 727 BTU/hr
6. heat flux = 727/0.551 = 1320 BTU/hr sq. ft
7. heat input per inch of tube = $\frac{727}{35.55} = 20.45 \frac{BTU}{hr\ in.}$
8. heat capacity rate = $Wc + W_s c_s = 18.89$ BTU/hr F
9. mixture temperature rise per inch = $\frac{20.45}{18.89} = 1.08 \frac{F}{in.}$
10. measured inlet mixture temperature = 70.7 F
11. mixture temperature at 6" = $6 \times 1.08 + 70.7 = 77.2$ F
12. measured average tube wall temperature = 204.3 F
13. temperature difference = 204.3 - 77.2 = 127.1 F
14. heat transfer coefficient = $\frac{(\text{item 6})}{(\text{item 13})} = \frac{1320}{127.1} = 10.38 \frac{BTU}{hr\ ft^2\ F}$
15. local Nusselt number = $\frac{hD}{k} = 38.4$

Nusselt numbers at the remaining locations were computed in the same way.

Friction factor calculation

Friction factors were computed according to the equation derived in Appendix D. For the same run as used previously, the procedure is as follows:

1. total mass rate = 29.0 + 62.5 = 91.5 lb/hr
2. mass velocity, $G_m = \frac{91.5}{2.76} \times 10^{-3} = 3.32 \times 10^4$ lb/hr. ft^2
3. $G_m^2 = 1.102 \times 10^{10}$ (lb/hr ft^2)^2
4. mixture temperature at 18 in. $T_{av} = 549.9$ R
5. $\frac{(\frac{Ws}{W} + 1)\, g}{G_m^2\, R\, T_{av}} = 4.075 \times 10^{-5}$ $(ft^2/lb)^2$

   (R = 53.3 ft/R, $g = 4.17 \times 10^8$ ft/hr^2
6. measured inlet pressure = 2058 psfa
7. measured pressure drop = 6.2 psf
8. $P_1^2 - P_2^2 = (2P_1 - \Delta P)\, \Delta P = 4109$ $(psf)^2$

9. $\dfrac{\left(\frac{W_s}{W} + 1\right) g}{G_m^{\,2} R T_{av}} \left(P_1^{\,2} - P_2^{\,2} \right)$ = (item 5) (item 8) = 1.035

10. measured inlet temperature, T_1 = 530.4 R

11. calculated mixture outlet temperature, T_2 = 566.2 R

12. $\dfrac{P_1 T_2}{P_2 T_1} = \dfrac{\text{(item 6) (item 11)}}{\text{(item 6 + item 7)(item 10)}}$ = 1.069

13. 2 (ℓn of item 12) = 0.134

14. $\dfrac{4fL}{D}$ = (item 9) - (item 13) = 0.901

15. f = $\dfrac{\text{(item 14)}}{203}$ = 0.00445

ACKNOWLEDMENTS

The author wishes to express his appreciation to Professor Leonard Farbar for his continued interest and support throughout the course of this program, to Professor R. A. Seban for his valuable suggestions and comments, and to Professor E. E. Petersen for his review and comments on the thesis.

The author further wishes to thank for their assistance in the experimental work: Messrs. Richard Brock and William Asakawa for their help in equipment operation and data reduction; Messrs. A. W. Cauwenbergh, F. W. Moore, and W. F. Pemberton for their help in the fabrication and installation of the apparatus.

Above all, this work is dedicated with love and gratitude to my wife, Lois, for her constant patience and understanding during countless evenings and weekends, while this dissertation was being prepared.

REFERENCES

1. Babcock and Wilcox Co., Gas Suspension Coolant Project, AEC contract No. AT(30-1) 2316, Final Report No. BAW-1159 (1959).
2. R. G. Deissler, Analysis of turbulent heat transfer, mass transfer and friction in smooth tubes at high Prandtl and Schmidt numbers, NACA TN 3145, 1954.
3. C. A. Depew, Heat Transfer to Flowing Gas-Solids Mixtures using Solid Spherical Particles of Fixed Size, MS Thesis in Mechanical Engineering, University of California, 1957.
4. L. Farbar and M. J. Morley, Heat Transfer to Flowing Gas-Solids Mixtures in a Circular Tube, Ind. Eng. Chem. Vol. 49, 1957 p. 1143-50.
5. James P. Hartnett, Experimental Determination of the Thermal Entrance Length for the Flow of Water and Oil in Circular Pipes, Trans ASME, Vol. 77, 1955, p. 1211-1220.
6. John L. Lumley, Some Problems Connected with the Motion of Small Particles in a Turbulent Fluid, PhD Thesis in Aeronautics, Johns Hopkins University, 1957.
7. William H. McAdams, Heat Transmission, 3rd ed., McGraw-Hill, New York, 1954, p. 210.
8. William H. McAdams, ibid, p. 156.
9. Hans Meyer, Allgemeine Gesetzmässigkeiten bei der pneumatischen Forderung, Doktor Ingenieurs Dissertation, Rheinisch - Westfalischen Technischen Hochschule, Aachen, Germany, 1959.
10. J. R. Nilson, Elimination of Electrical Interference in High Temperature Thermocouple Installations, presented at Summer-Instrument and Automation Conference and Exhibit of the Instrument Society of America, preprint number 36-SF 60, San Francisco, May 1960.
11. Richard L. Peskin, Some Effects of Particle-Particle and Fluid Particle Interaction in Two-Phase Flow Systems, to be presented at the Heat Transfer and Fluid Mechanics Institute, Stanford University, (1960).

12. J. R. Sellars, M. Tribus, and J. S. Klein, Heat Transfer to Laminar Flow in a Round Tube or Flat Conduit-The Graetz Problem Extended, Trans. ASME, Vol. 78, 1956, p. 441-8.

13. R. Siegel and E. M. Sparrow, Comparison of Turbulent Heat-Transfer Results for Uniform Wall Heat Flux and Uniform Wall Temperature, Trans. of ASME Journal of Heat Transfer, May 1960, p. 152-3.

14. C. A. Sleicher, Jr. and M. Tribus, Heat Transfer in a Pipe with Turbulent Flow and Arbitrary Wall Temperature Distribution, Trans. ASME, Vol. 79, 789-798 (1957).

15. S. L. Soo, Statistical Properties of Momentum Transfer in Two Phase Flow, Chemical Engineering Science, Vol. 5, April 1956, p. 56-67.

16. S. L. Soo and H. K. Ihrig, Jr., Experimental Determination of Statistical Properties of Two-Phase Turbulent Motion, Project Squid Technical Report PR-82-P, August, 1958.

17. S. L. Soo and Chang-Lin Tien, Effect of the Wall on Two-Phase Turbulent Motion, Journal of Applied Mechanics.

18. E. M. Sparrow, T. M. Hallman, R. Seigel, Turbulent heat transfer in the thermal entrance region of a pipe with uniform heat flux, Appl. Sci. Re., Section A, Vol. 7, p. 37, (1957).

19. C. L. Tien, On the eddy diffusivities for momentum and heat, Appl. Sci. Res. Section A, Vol. 8, p. 345, (1958).

20. Chang-Lin Tien, Heat Transfer to a Turbulently Flowing Fluid-Solid Mixture in a Pipe, to be presented at the Fourth National Heat Transfer Conference at Buffalo, New York, Aug. 1960.

21. M. Tribus and J. Klein, Forced Convection from Non-Isothermal Surfaces, Heat Transfer Symposium, Univ. of Michigan 1952, p. 211-36.

22. Vito A. Vanoni, En-Yun, R. W. Davies, Dynamics of Particulate Matter in Fluid Suspensions, California Institute of Technology Sedimentation Laboratory Report No. N-71.1, Nov. 1950, p. 9.

23. T. Yuge, "Experiments on Heat Transfer from Spheres Including Natural and Forced Convection". Paper No. 59-A-123 Heat Transfer Division Annual Meeting ASME Atlantic City, N. J. 1959.